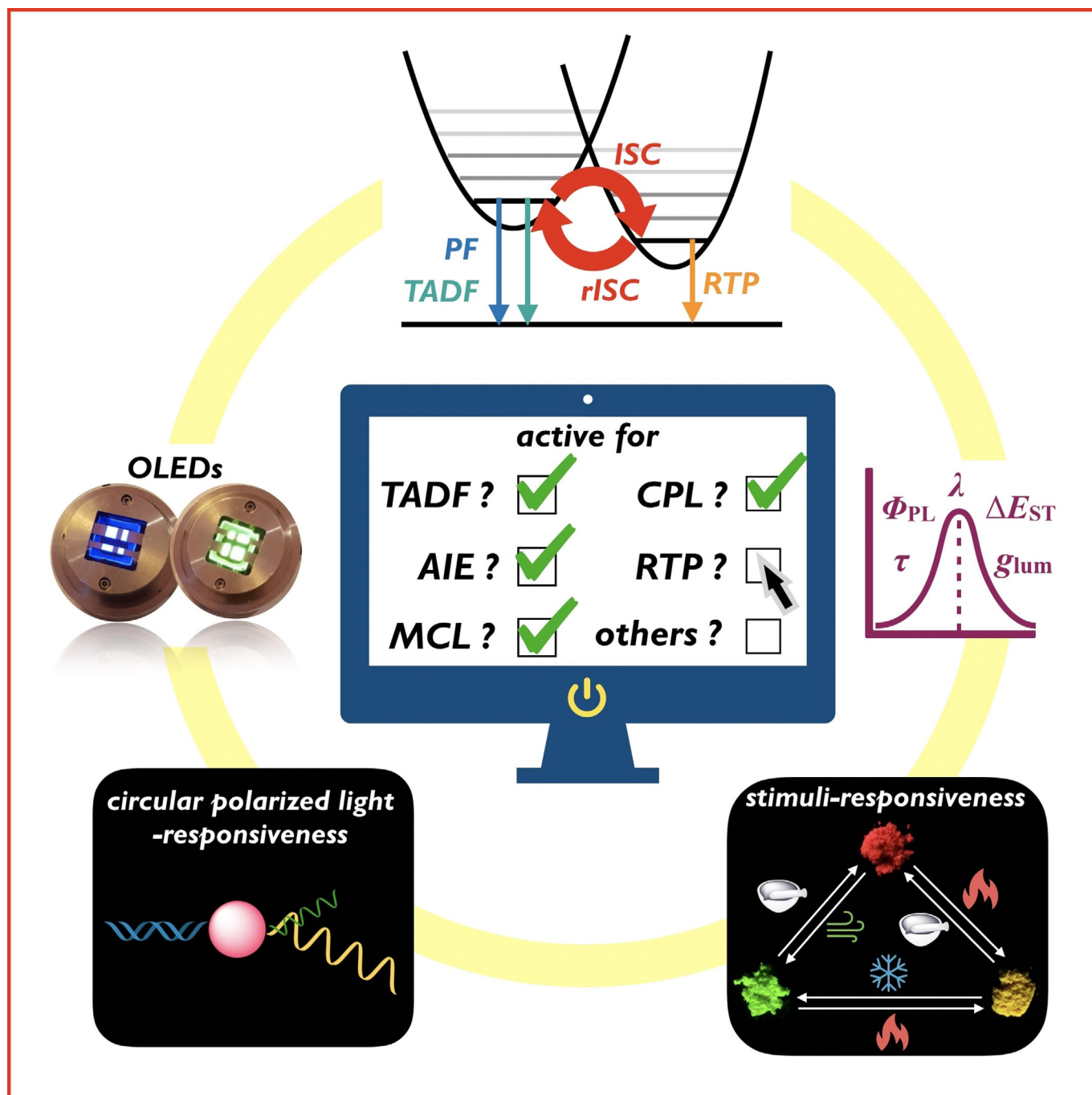


SPECIAL ISSUE
Recent Advancements in and the Future of Organic Emitters: TADF- and RTP-Active Multifunctional Organic Materials

Przemyslaw Data^{*[a, b]} and Youhei Takeda^{*[c]}



Abstract: Organic emitting compounds that are based on π -conjugated skeletons have emerged as promising next-generation materials for application in optoelectronic devices. In this Minireview, recent advances in the development of organic emitters that irradiate room-temperature phosphores-

cence and/or thermally activated delayed fluorescence with extraordinary luminescence properties, such as aggregation-induced emission, mechanochromic luminescence, and circularly polarized luminescence, are discussed.

1. Introduction

Since the origins of life, the need for light has been a feature of our existence and survival. Light is used in many processes in biological systems: it not only helps plants to produce oxygen that is needed for life through photosynthesis, but also animals to develop sight. First, humans tried to understand the science of fire and the light that is generated from it: how to produce and harvest this new type of energy. Firelight became used in the form of oil or gas lamps, but that was not enough. Scientists began to search for new ways to obtain “clean” light. In this regard, the “father” of the next breakthrough was Edison and his light bulb. Although there is ongoing debate whether or not he was its original inventor, he was the first person to commercialize this technology on a global scale. However, again, harvesting light inside glass bulbs was not enough, and scientists tried to understand the underlying processes behind this light source. To help understand what is going on inside such electrically excited materials, quantum theory was developed, which made it possible to create sources of light with an entirely different mechanism of stimulating atoms or molecules than ever before. It turned out that the mechanism that happens in an incandescent light bulb is the

same as that in oil or gas lamps and, in both cases, a large amount of heat is generated as waste energy. Later, the “cold” method to produce light was discovered and used in fluorescent lamps. This method is based on the collision of electrons with mercury vapor atoms, which allows the temperature of the light source to be lowered and offers higher efficiencies than “hot” methods. The next boost came through the discovery of electroluminescence, in which the recombination of charge carriers in inorganic solid silicon carbide was applied to obtain efficient emission.^[1] Without those discoveries, it would not have been possible to develop new types of emitters, that is, organic emitters. Organic substances have attracted the attention of scientists as a light source owing to their excellent luminescence properties and their highly efficient light radiation within the visible spectrum. Organic dye lasers, first developed in 1967,^[2] not only generate strong pulses and continuous light beams, but can also be tuned to a wide range of radiation wavelengths. As such, it is unsurprising that such organic compounds have also been used as more conventional sources of light in electroluminescence, a process in which matter is excited by using a current or an electric field. The first organic light-emitting diodes (OLEDs) exhibited low efficiencies for the conversion of electricity into light, because the injection of charge into organic crystals required relatively high voltages.^[3]

As you can see, the development of light sources has been a bumpy road, but today, light and its sources are a ubiquitous part of human existence: from the sun to artificial light sources, such as TVs, smartphones, and light-up advertisements. Furthermore, we also encounter organic materials in daily life in various forms, for example, in prototypical and commercial chemical sensors, photovoltaic cells, and active matrix organic light-emitting diode (AMOLED) displays. The major advantage of organic emitters is the ability to tailor their properties, including their emission color, by modifying their molecular structure.

Before an organic molecule emits photons, it must be electronically excited in some way, the easiest of which is to provide an amount of energy that corresponds to the difference between its ground state (S_0) and its first excited state (S_1 ; or one of the higher excited states). In such a transition ($S_0 \rightarrow S_1$), one of the two electrons in the HOMO of the molecule is transferred to the LUMO. The two electrons in the HOMO must have opposite (i.e., antiparallel) directed electron spin momentum (or spins). Therefore, the total spin number is 0 and this basic state is called the singlet state, or “singlet”. Because a photoabsorption transition typically retains the spin, in the S_1 excited state, both electrons also have antiparallel spins. The

[a] Prof. Dr. P. Data
Faculty of Chemistry
Silesian University of Technology
M. Strzody 9
44-100 Gliwice (Poland)
E-mail: przemyslaw.data@polsl.pl

[b] Prof. Dr. P. Data
Center of Polymer and Carbon Materials
Polish Academy of Sciences
M. Curie-Skłodowskiej 34
41-819 Zabrze (Poland)

[c] Prof. Dr. Y. Takeda
Department of Applied Chemistry
Graduate School of Engineering
Osaka University
Yamadaoka 2-1, Suita
Osaka 5650871 (Japan)
E-mail: takeda@chem.eng.osaka-u.ac.jp

 The ORCID identification number(s) for the author(s) of this article can be found under:
<https://doi.org/10.1002/asia.201801791>.

 © 2019 The Authors. Published by Wiley-VCH Verlag GmbH & Co. KGaA. This is an open access article under the terms of the Creative Commons Attribution Non-Commercial NoDerivs License, which permits use and distribution in any medium, provided the original work is properly cited, the use is non-commercial and no modifications or adaptations are made.

 This manuscript is part of a special issue on π -Conjugated Compounds for Molecular Materials. Click here to see the Table of Contents of the special issue.

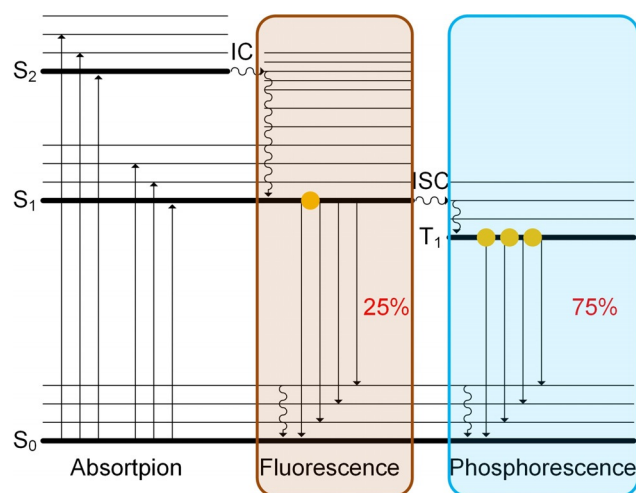


Figure 1. Jablonski diagram for absorption, fluorescence, and phosphorescence. S₀ denotes the ground state; S₁ and S₂ denote the first and second excited singlet states, respectively; T₁ denotes the first excited triplet state. The following conversion routes are possible: internal conversion (IC) and intersystem crossing (ISC).

photophysical processes that occur after the excitation can be described by a Jablonski diagram (Figure 1).

When the excitation energy is converted into the motion energy of nucleus oscillation, the molecule quickly (on the order of $\times 10^{-14}$ to $\times 10^{-11}$ s) reaches the lowest oscillation level of the excited state (S₁). A typical organic molecule stays in this S₁ state for a few nanoseconds ($\times 10^{-9}$ s), before returning to the S₀ state by emitting a photon or by deactivation through nonirradiative pathways. The emission of a photon from the S₁ state is called fluorescence. When a particle is in the S₁ state, the mutual orientation of the spins of the two electrons can change—from antiparallel to parallel. Through this process, known as intersystem crossing (ISC), the S₁ state can be converted into the triplet state (or “triplet”, T₁), in which the total spin number is 1. For a typical organic molecule, owing to the low probability of the transition to the ground state, the particle can stay in the triplet state for a long lifetime (from ms to s). Therefore, the triplet state is regarded as a “sink” for excitons. The emission of a photon from the triplet state is called phosphorescence. In most organic molecules, it is possible to emit phosphorescence at low temperatures (below 100 K) by eliminating the possibility of thermal nonradiative deactivation pathways from the T₁ state. Until about 10 years ago, scientists were sure that phosphorescence at room temperature would only be possible if heavy atoms were present in the molecule, such as heavy metal complexes in which there is strong coupling between the singlet and triplet states.

Today, both processes (fluorescence and phosphorescence) are widely used in commercial OLEDs, and a broad range of organic compounds have been utilized as emitters. One important feature of π -conjugated organic emitters in OLEDs is their high electroluminescence efficiencies. Currently, there is great demand for blue OLEDs, because there are very few such organic emitters that simultaneously realize high efficiencies and

appropriate lifetimes.^[4,5] Furthermore, blue light can also be transformed into red and green light through internal or external color-conversion processes, which would simplify the fabrication of RGB OLEDs, thereby allowing for their large-scale manufacture to cut product costs.^[6] To optimize the operation of OLEDs based on π -conjugated emitters, a balanced distribution of injected charge carriers (i.e., holes and electrons) is required, which ensures the effective recombination of holes and electrons, thereby significantly improving the OLED efficiency.^[7,8] Conversely, the use of organic materials with a large energy gap, high ionization potential, or low electron affinity often leads to the disruption of the desired equilibrium. These parameters can be controlled by adjusting the length of π -conjugation in the molecule or by introducing electron-donating or -accepting substituents into the luminophores.^[9] A significant change in the structure of organic π -conjugated compounds can also cause variation in their electronic and photo-physical properties.^[10,11] In summary, there are many factors that have to be taken into account in the design of organic emitters, and even a slight change in any of these factors can influence other parameters. Therefore, it is necessary to understand the background of the emission processes in OLEDs in greater detail before designing new organic emitters.

2. RTP and DF in Organic Emitters

OLEDs are typically divided into fluorescence- and phosphorescence-emitting devices. Fluorescence is a fast relaxation pro-

Przemyslaw Data is currently a Professor at the Silesian University of Technology (Poland). Prof. Data received his Ph.D. with honors in Chemistry in 2013 from the Silesian University of Technology (Poland), and his work received the Polish Prime Minister’s award for the Outstanding Doctoral Dissertation. After completing his Ph.D., he received Mobility Plus funding, followed by a Marie Skłodowska-Curie Individual Fellowship to undertake scientific work in the area of TADF emitters at Durham University (UK), which earned him the MIT Innovator Under 35 award (2017 Polish Edition). His current research interests include the design and analysis of organic small molecules and polymeric materials for application in organic electronics.



Youhei Takeda received his Ph.D. in Organic Chemistry in 2010 from Kyoto University (Japan). Then, he worked as a JSPS Research Fellow (PD) at Massachusetts Institute of Technology (USA). He is currently an Associate Professor at Osaka University (Japan) and an Adjunct Lecturer at Vietnam–Japan University (Vietnam). He was awarded Incentive Award in Synthetic Organic Chemistry, Japan in 2018. His current research interests include the design, synthesis, and optoelectronic application of heteroatom-embedded exotic π -conjugated organic emissive materials.



cess in which an excited molecule in the excited singlet state returns to the ground state by emitting energy in the form of photons (Figure 1). Phosphorescence is a longer relaxation process that is associated with a radiative transition from the molecular excited triplet state to the singlet ground state. Such a transition is forbidden, but mixing of the triplet and singlet wave functions affords very weak long-lived radiative decay, which is mediated by ISC. Because charge recombination in the OLED statistically creates excited states at a ratio of one singlet to three triplet excitons, the quantum efficiency of a fluorescent emitter device will, therefore, be limited to 25%, which means that the 75% of triplet excitons will be lost. The first-generation OLED emitters were only fluorescence emitters and, hence, their final device efficiencies were quite limited. To increase their efficiencies, phosphorescence emitters were implemented, which enabled an internal quantum efficiency of almost 100% by harvesting both the triplet and singlet excited states (Figure 2a). The main problem with phosphorescence emitters is that they are heavy metal complexes; in many cases, very expensive and scarce iridium complexes were used. There are two ways to remove heavy metal complexes from

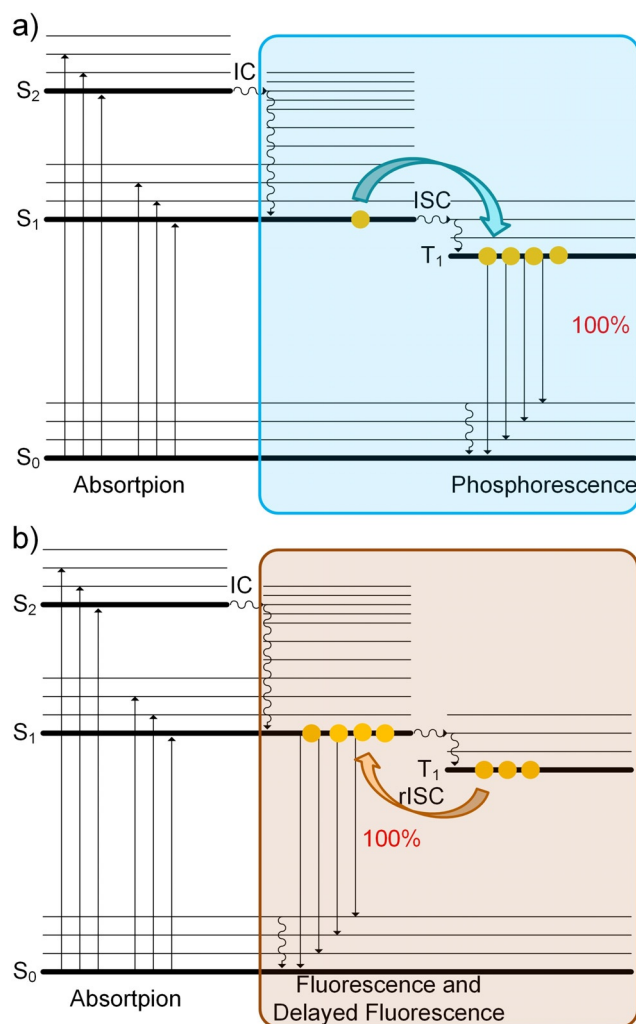


Figure 2. Jablonski diagram for the processes that are involved in a) phosphorescence-based emitters and b) delayed-fluorescence-based emitters.

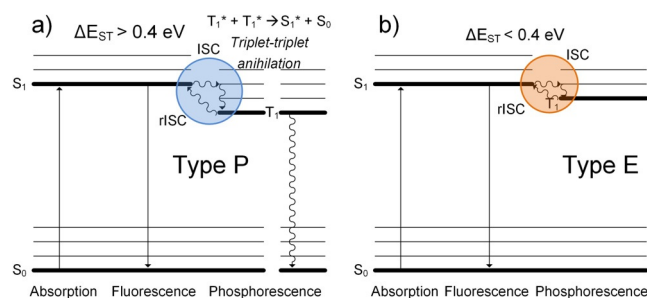


Figure 3. Jablonski diagram for delayed fluorescence: a) P-type delayed fluorescence with triplet fusion and b) E-type delayed fluorescence. ΔE_{ST} = singlet-triplet energy difference.

OLED emitters: 1) to employ room-temperature phosphorescence (RTP) emission and 2) to use delayed fluorescence (DF) processes (Figure 2b and Figure 3).

RTP and DF are theoretically opposite processes: RTP is more efficient at lower temperatures, whereas DF is not. To observe delayed fluorescence, we need to increase molecular vibration by adding thermal energy to accelerate reverse intersystem crossing (rISC) from the local triplet state to the singlet state, which is supported by inter- or intramolecular charge transfer. As for the phosphorescence process, owing to its long lifetime, it is necessary to cool the molecule to eliminate the possibility of nonradiative deactivation from the T₁ state. Researchers from Princeton University and the University of Southern California employed the phenomenon of transfer of excitation energy between molecules and used phosphorescent heavy metal complexes that absorbed the triplet excitons and converted it into light. In such phosphorescent organic light-emitting diodes (PHOLEDs), which employed organometallic complexes as emitters, it was possible to overcome this problem and decrease the phosphorescence lifetime to microseconds through a metal-to-ligand charge transfer (MLCT) process^[12–14, 16–19] and a degenerate d orbital.^[12, 13, 15] MLCT involves electron or charge transfer from molecular orbitals with metal-like character (e.g., d orbitals in these cases) to those with ligand-like character that have low-lying π^* orbitals. Moreover, such metal-ligand interactions can induce an electrostatic field, which breaks the spin degeneracy of two or more unpaired electrons in a metal complex in the absence of a magnetic field, known as zero-field splitting (ZFS). ZFS is an important factor in obtaining strong spin-orbit coupling of metal complexes and for observing RTP.^[12, 13, 19–21] To obtain a similar effect at room temperature without the use of organic compounds with a metallic center (i.e., organometallic complexes), new approaches for designing RTP-active organic compounds are required.

DF also allows almost 100% internal quantum efficiency to be obtained from a triplet exciton, without the need for an iridium phosphorescent dopant. In this case, a molecule is first excited to the triplet state, then returns to the singlet excited state and relaxes to the ground state by emitting photons. There are two types of DF. The first is P-type delayed fluorescence (P-DF; Figure 3a), named after pyrene as the first compound with which this type of DF was observed.^[22, 23] In this

process, two excited triplet states from adjacent molecules annihilate each other to leave one molecule in the ground state and the other in the excited singlet state (this process is also called triplet fusion, TF, or triplet-triplet annihilation, TTA). The main disadvantage of this process is its low maximum internal quantum efficiency (20–50%). The mechanism for P-type delayed fluorescence can be described as in Equations (1)–(4).



The second type of DF is eosin-type delayed fluorescence (E-DF), or thermally activated delayed fluorescence (TADF; Figure 3b).^[23] For this process to occur, the excited singlet and triplet states must have very similar energies. In this case, the molecule is able to move from a triplet excited state back to the singlet excited state through thermal activation and reverse intersystem crossing (rISC). Then, the molecule in the excited singlet state relaxes by emitting a photon. The maximum internal quantum efficiency of this process is 100%. The mechanism for E-type delayed fluorescence can be described as in Equations (5)–(8).



PHOLED devices can achieve almost 100% internal quantum efficiency, whereas typical OLED systems, which are based on fluorescent emitters, only have a maximum efficiency of 25%. E-type DF offers 100% efficiency for optoelectronic systems. Delayed fluorescence is a non-collisional energy-transfer process that exhibits the characteristic fluorescence emission spectrum, but its lifetime is consistent with iridium phosphors. Various types of emissive states can be created in OLEDs.^[24,25] In organic solids that are composed of chemically identical molecules, which do not aggregate in the ground state, the formation of an excimer excited state is possible, owing to resonance interactions between a molecular exciton and a neighboring molecule in its ground state. Excited state intramolecular charge transfer is a fundamental process that occurs in several natural systems and is a key mechanism in photochemistry and photobiology. The absorption of photons by molecules that contain both donor and acceptor moieties separated by a spacer group triggers charge transfer from a donor to an acceptor in the excited state, which leads to the formation of an internal charge transfer (ICT) state and the emission occurs from both the locally excited (LE) state and the ICT state.^[27–29] Emission from the ICT state is observed in all TADF

guest–host-type emitters, whereas, in bicomponent systems of electron donor (D) and electron acceptor (A) molecules, the formation of exciplex states through electron transfer from the donor to the acceptor is highly facile. The molecular excitons can be viewed as neutral correlated electron–hole (e–h) pairs with an interchange mean separation that is less than the intermolecular spacing, whilst the size of bimolecular (B–M) excited states typically corresponds to one or two times the intermolecular spacing. The molecular and B–M excited states can either be generated optically by using light or electrically through electron–hole recombination and they appear in both photoluminescence (PL) and electroluminescence (EL), respectively.^[26,30]

Research on the materials and devices that employ the TADF mechanism is still in its infancy. Of course, hundreds of devices have been reported in the literature, and several different mechanisms have been described, but more work is needed to unify all of this information and reach beyond our current knowledge. TADF emitters, which comprise an electron-donating (D) group and an electron-accepting (A) group, are characterized by a very small gap between the singlet and triplet states.^[31] A small range of TADF materials and devices have been reported, such as **4CzIPN**^[32] and **DPTZ-DBTO2**,^[33] with very high external quantum efficiencies (EQEs) of up to 19% (Figure 4). This result is indicative of efficient triplet harvesting and confirms that 100% internal quantum efficiency is possible. Importantly, these devices have a very simple “stack” structure that is typically comprised of three–five organic layers, without the need for a p–i–n structure (p-type semiconductor, intrinsic semiconductor, and n-type semiconductor, respectively).^[34] These devices also have ultralow turn-on voltages of the order of 2.7 V. Initial studies on the photophysics of TADF systems have shown the importance of the $n\pi^*$ excited

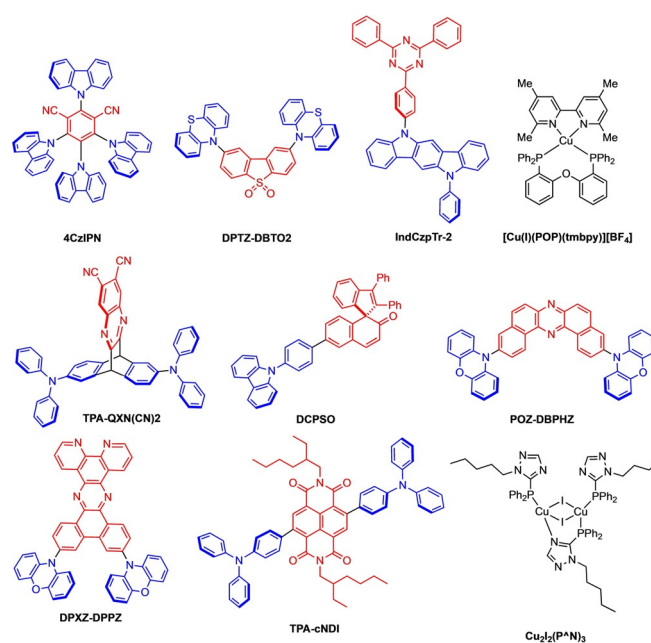


Figure 4. Examples of TADF emitters. Electron-donating groups are shown in blue; electron-accepting groups are shown in red.

state in heteroatom-containing π -conjugated compounds,^[35] the critical role of the triplet levels in the system,^[36] and the very low (< 50 meV) energy gaps in the charge-transfer states.^[37] From the viewpoint of the TADF mechanism, to develop an efficient emitter, firstly the singlet and triplet excited states must be located close to each other (< 200 meV) to allow for efficient rISC. When the molecule in a triplet excited state is thermally excited to a higher vibronic level that matches a level in the singlet excited state, rISC should occur.^[37,38] Unexpectedly, it was observed that the emitting dipoles in these systems are partially aligned and that such anisotropic emission gives rise to a light outcoupling factor. Devices with external quantum yields of > 30% have been fabricated by using compound **IndCzpTr-2** (Figure 4).^[39] However, this process is not simple and, in fact, a very recent finding from Durham University showed that the charge-transfer (CT) state must couple to a local (D or A) triplet state through spin-orbit coupling, and that the widely quoted idea of ^1CT - ^3CT spin-orbit coupling (SOC) interexchange is incorrect, because it is a forbidden process. The ICT process of the excited molecules is affected by several environmental factors, including polarity, viscosity, and hydrogen-bonding interactions.^[40,41] A red shift of the CT emission is observed with increasing solvent polarity. In some cases, this shift can allow the observation of the TADF emission in highly polar solvents for compounds with larger singlet-triplet gaps, because the local triplet level is not shifted in energy by polarity. This process is quite useful when solution-based hosts are used. Conversely, in the solid state, it is difficult to properly describe the polarity of the host and its influence on the ICT state of the TADF emitter. The rigidity of the host is important, because the vibration of the TADF emitter affects the emission: when the molecule is frozen, only a mixed emission of the fluorescence and phosphorescence is observed, rather than TADF. Another important factor for TADF emission is the morphology of the host. We observed a strong influence of the glass transition of the host on the rISC process. As presented by Adachi and co-workers, the emitter had to be annealed below the glass-transition temperature of *N,N'*-dicarbazolyl-4,4'-biphenyl (CBP; ca. 62 °C) when solution processing was used.^[42] CBP is one of the most used hosts for green-orange emitters, owing to the influence of glass transition on the formed devices. During normal operation, the temperature inside the pixel cell is higher than 62 °C, which means that the glass transition of the host could be a factor in diminishing the device efficiency and causing a roll-off effect. These aspects along with many others have not yet been fully explained and are important for the development of ICT-based TADF devices.

The TADF mechanism has been shown to be a promising way of harvesting triplets at almost 100% efficiency without the use of iridium-based complexes. However, many questions remain: what design rules lead to the generation of emitters at specific wavelengths? The majority of emitters emit green and yellow light, whereas there are insufficient efficient emitters of red and blue light. How can we control the emission bandwidth? For applications in lighting, we need broad white-light emission, whereas for displays, narrow emission is needed.

How can we fabricate TADF emitters and devices that are stable? The efficiencies of TADF devices are still much lower than those of commercial organometallic complexes, mainly owing to the long-lived excited state in TADF emitters. TADF emitters typically cover the green–yellow region, including **4CzIPN**,^[32,43] **DPTZ-DBTO2**,^[33] **[Cu^I(POP)(tmbpy)][BF₄]**,^[44] and **TPA-QXN(CN)₂**,^[45] and there have been reports of efficient blue TADF systems, but their stability is limited.^[46–48] There are not many reports of orange-to-red TADF emitters and they are mainly based on anthraquinone^[49] spironaphthalenone (**DCPSO**),^[50] phenazine (**POZ-DBPHZ**)^[51] and **DPXZ-BPPZ**,^[52] or naphthalenediimide (**TPA-cNDI**)^[53] acceptors (Figure 4). The problem with red TADF emitters is fluorescence quenching and the difficulty of distinguishing between the TTA and TADF mechanisms, owing to the small energy differences.

There are hundreds of examples of phosphorescent organometallic complexes and thermally activated delayed fluorescent organometallic complexes and fully organic compounds, but they always exhibit delayed emission through one of those pathways, phosphorescence or delayed fluorescence. Typically, if there is efficient TADF, the phosphorescence is much weaker. A newer approach is to use TADF emitters as hosts for phosphorescence emitters. According to literature reports, the TADF hosts stabilize the charge-transfer state and the final devices exhibit smaller roll-offs, which allows the formation of stable white-emissive devices.^[54–59] Moreover, theoretically, TADF molecules should be good hosts for blue phosphors, because their small ΔE_{ST} gap can improve the FRET to the S_1 energy level of the dopants, but can also dynamically adjust the singlet and triplet exciton allocation through a balance of ISC–rISC (Figure 5). Such behavior is beneficial for suppressing concentration quenching and efficiency roll-offs.^[59]

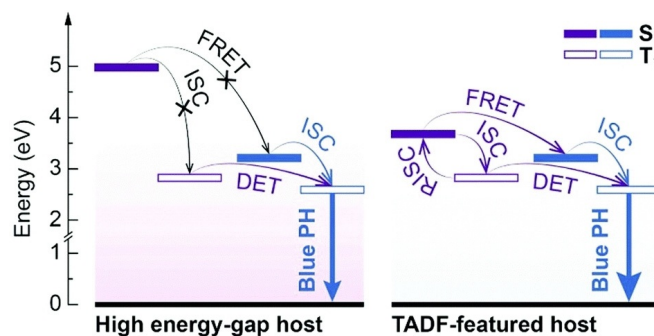


Figure 5. Comparison of the energy transfer and transition processes in conventional high-energy-gap hosts and TADF-featured hosts for blue phosphors. FRET = Förster resonance energy transfer, DET = Dexter energy transfer, PH = phosphorescence. Reproduced with permission from Ref. [59]. Copyright 2018, Royal Society of Chemistry. Recently, there was a report of organometallic compounds that exhibited both TADF and RTP processes. The Yersin group synthesized copper complex **Cu₂I₂(P[^]N)₃** (Figure 4),^[60] but the problem of using organometallic complexes remained.

3. Metal-Free RTP Emitters

Recently, there have been several reports on the RTP effect in metal-free small organic molecular compounds.^[61] However,

despite these advances, all attempts to create a stable, efficient OLED device have failed. Although there have been some examples of RTP in OLEDs, the contribution is very low. The approach to design such molecules is similar to that for TADF emitters, but, for phosphorescence, the donor and acceptor molecules cannot communicate and the angle between the planes needs to be frozen. To stop the vibration, Bryce and co-workers developed **DBTZ-DBTO2** derivatives,^[62] whilst the Penfold and Dias groups developed **DPTZ-DBT** derivatives (e.g., **DPTZ-Me-DBT**; Figure 6),^[63,64] by adding side groups as steric

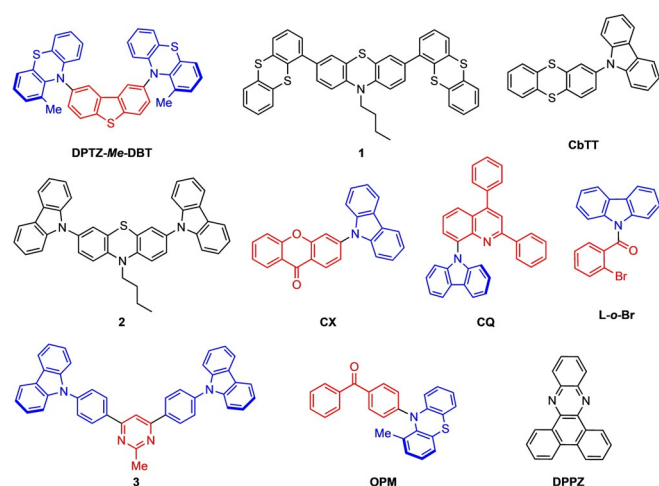


Figure 6. Examples of RTP compounds. Electron-donating groups are shown in blue; electron-accepting groups are shown in red.

hindrance. By freezing the rotation and quenching the TADF process, RTP emission can be observed. Thereafter, several similar approaches were developed, but the main concept remains the same, to try to use ICT, instead of MLCT, to speed up the phosphorescence lifetime, but also to decrease the possibility of the opposite TADF process by freezing the rotation between the donor and acceptor planes. On the other hand, there have been some examples of fully organic RTP emitters that didn't possess steric hindrance in the structure, or the side groups were big enough to slow the motion sufficiently to observe RTP phosphorescence emission at higher temperatures. Several examples of RTP compounds that contain thianthrene and phenothiazine were reported by Pander et al. (e.g., **1**, **CbTT**, and **2**),^[65–67] whilst Zhang and co-workers reported a D–A-type xanthone-cored RTP compound (**CX**; Figure 6).^[68]

A similar approach for the design of new RTP molecules with the typical orange–red RTP emission has recently been developed. Carbazole–quinoline derivatives (**CQ**), first developed by Bhattacharjee et al.,^[69] exhibited dual TADF/RTP and orange RTP emission properties by applying a similar steric hindrance effect to that presented by Penfold and Dias.^[64] Liu et al. observed the possibility of controlling the triplet-harvesting process and enhancing the RTP in the solid state by forming regioisomeric macrocrystal structures of *N*-benzoyl-carbazole derivatives (e.g., **L-o-Br**; Figure 6).^[70] RTP was also observed in pyrimidine derivatives by Serevičius et al., in which

differently substituted carbazole–pyrimidine-cored derivatives were analyzed (e.g., **3**; Figure 6).^[71] The influence of the different conformers allowed both RTP and TADF to be observed, but no correlation between a particular structure and the emissions was presented.^[71] The influence of conformation on the photophysical properties of organic molecules and their stabilization through steric hindrance was presented by Bryce and co-workers,^[72] in which the analysis of different phenothiazine-benzophenone compounds was demonstrated. By adding a methyl group to the phenothiazine donor (**OPM**), the molecules adopted a quasi-axial conformation in the crystal (Figure 7), which enhanced the RTP process. In contrast, when a methyl group was connected to the acceptor (**OMP**), the molecules adopted a quasi-equatorial conformation (Figure 7), which enhanced the TADF emission.^[72]

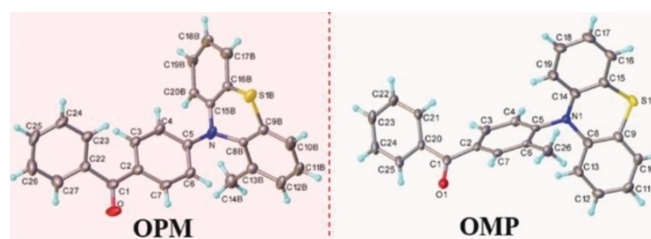


Figure 7. Conformations of **OPM** and **OMP** in the single crystals. Adapted from Ref. [72].

More recently, phenazine derivative **DPPZ** (Figure 6) was synthesized by Zhou et al. as an example of a dual-phosphorescence emitter that could be used as single-molecular white-light emitter (Figure 8).^[73] In their work, the authors summarized information found in the literature and assumed that, to

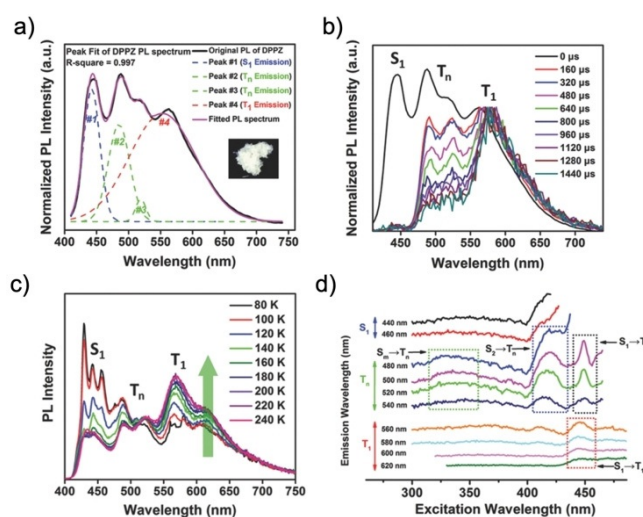


Figure 8. RTP properties of **DPPZ** as a neat powder: a) PL spectrum and peak fitting under ambient conditions. b) Normalized time-resolved PL spectra; the spectra were normalized to the T_1 emission for the purpose of comparison. c) Temperature-dependent PL spectra within the range 80–240 K. d) Excitation spectra of **DPPZ** at different emission wavelengths ($\lambda = 440$ –620 nm). The spectra shown in (a) and (b) were normalized to ensure that the results were comparable. Adapted from Ref. [73].

achieve efficient RTP in pure organic materials, two key countermeasures should be adopted: 1) accelerate the ISC process for the adequate generation of triplet excitons; and 2) suppress the nonradiative deactivation of triplet excitons.^[73] Moreover, the authors claimed that some light heteroatoms could also play a similar role to heavy atoms, which provided a lone pair of electrons to strengthen SOC and to facilitate ISC between $n \rightarrow \pi^*$ and $\pi \rightarrow \pi^*$ character states, according to the El-Sayed rule.^[73]

As a short summary, the design principle for RTP-emissive fully organic compounds seems to be quite similar to that for TADF-active emitters: CT character is quite important and SOC is crucial for efficient triple generation, but the singlet–triplet gap must be much larger than TADF molecules to suppress rISC and shift the equilibrium to the triplet state.

4. Multifunctional Emitters

Nowadays, products are no longer “single use”. Instead, like with smartphones, for example, which contain multiple devices and offer a range of features, organic compounds also need to be multifunctional. However, it is not easy to design such multifunctional organic emitters, because changing one energy state would usually affect the other, which, in simple terms, may be described similarly to Newton’s third law: for every action, there is definitely a reaction, although it may not be equal and opposite reaction. This situation is also the case for RTP and TADF or mechanochromic luminescence (MCL)-active molecules. As discussed above, RTP and TADF are strictly opposite processes and, theoretically, if we have one, we should not have the other. However, in reality, we can sometimes observe the balance between these two processes. Why? The main reason is that conformers are involved in the photophysical processes. As reported by Takeda, Data, and co-workers^[107,109] and by Bryce, Dias, and co-workers,^[62,72] there is a strict correlation between the type of conformers or organic emitter and the resultant TADF or RTP process. Equatorial conformers of phenothiazine-containing D–A compounds can enhance TADF, whereas axial conformers enhance RTP (see below). Moreover, the conformers can be interchanged by adding energy through grinding, heating, or fuming (see below). This situation becomes even more complicated in the case of organic emitters that contain multiple conformationally flexible units (e.g., D–A–D-type structures with phenothiazine units).^[107] Furthermore, the luminescence properties of such multifunctional emitters are not only affected by temperature (RTP vs TADF emissions), pressure (MCL), and oxygen content (RTP/TADF vs quenching by molecular oxygen), but also by many other factors, such as the presence of ions, pH value in water-based systems, or even by the amount of light, which may simply interconvert the different conformers. Therefore, careful inspection of the photophysical properties of organic emitters is crucial to discovering their unique luminescent functions and thereby developing multifunctional emitters. The following sections will cover such TADF-active multifunctional organic materials.

4.1. TADF- and AIE-Active (AIDF) Materials

Organic emitters that not only show TADF but also aggregation-induced emission (AIE)^[74] (i.e., aggregation-induced delayed fluorescence, AIDF) hold great potential for efficient host-matrix-free (non-doped) OLED devices.^[75] Such non-doped OLEDs do not require tedious optimization processes, such as the selection of hosts or the control of dopant concentrations during the fabrication of the devices. In addition, the suppression of exciton quenching, such as single–triplet and triplet–triplet annihilation in AIDF OLEDs to decrease the efficiency roll-off is also beneficial. Therefore, AIDF-active compounds have emerged as promising organic emitting materials, especially in OLEDs.

In 2014, the Wang and Wang group developed donor–acceptor (D–A)-type TADF emitters that employed thioxanthone (TX) as an electron acceptor and triphenylamine (TPA) and *N*-phenylcarbazole (PhCz) as electron donors (Figure 9).^[76] Nota-

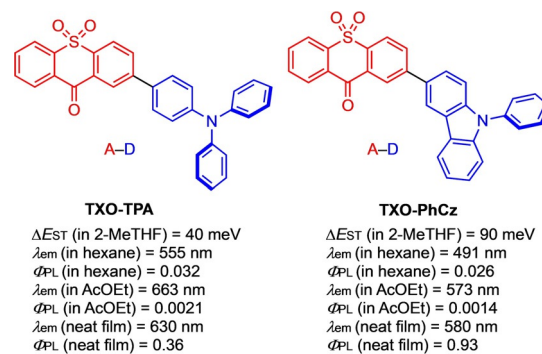


Figure 9. Molecular structures and photophysical data of TXO-TPA and TXO-PhCz. A = acceptor, D = donor.

bly, the intrinsic energy gap between the excited singlet (S_1) and triplet (T_1) states of TX was moderately narrow ($\Delta E_{ST} < 300$ meV), and structural modification of the TX core by introducing donor units allowed for further narrowing to < 100 meV, owing to effective separation of the HOMOs and LUMOs. Dilute solutions of TXO-TPA and TXO-PhCz showed very low photoluminescence quantum yields ($\Phi_{PL} < 0.05$). In sharp contrast, neat thin films of both compounds exhibited a dramatic increase in Φ_{PL} (0.36 and 0.93, respectively; Figure 9). Crystallographic analysis of both compounds suggested that the operation of intermolecular noncovalent interactions, such as $\pi \cdots \pi$ and C–H $\cdots\pi$ contacts, restricted the free rotations and vibrations in the molecules to suppress nonradiative thermal dissipation of the triplet excitons. OLED devices that were fabricated by using TXO-TPA and TXO-PhCz as emitters with the configuration ITO/PEDOT/TAPC/emitter doped in mCP (5 wt%)/TmPyPB/LiF (ITO = indium tin oxide, PEDOT = poly(3,4-ethylenedioxythiophene), TAPC = 4,4'-cyclohexyldienebis[*N,N*-bis(4-methylphenyl)benzenamine], TmPyPB = 1,3,5-tri(*m*-pyridin-3-ylphenyl)benzene) achieved high maximum external quantum efficiencies (EQEs) of 18.5% and 21.5%, respectively.

Thereafter, Chi, Zhang, Xu, and co-workers reported the synthesis of asymmetrical (D–A–D', **4**) and symmetrical (D–A–D, **5**) compounds that showed significant AIDF behavior (Figure 10a).^[77] According to X-ray crystallographic analysis of

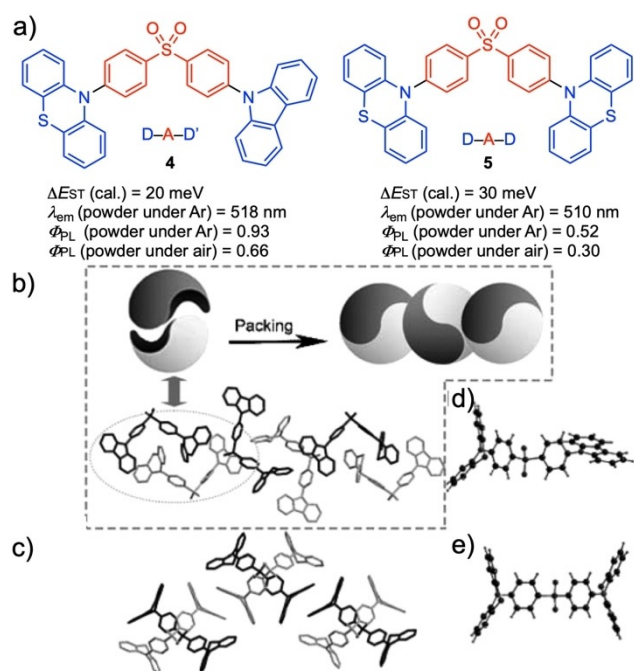


Figure 10. a) Molecular structures and photophysical properties of compounds **4** and **5**; b, c) packing structures of compounds **4** (b) and **5** (c); and d, e) molecular conformations of compounds **4** (d) and **5** (e), as determined by using X-ray crystallographic analysis. Adapted from Ref. [77].

single crystals of compounds **4** and **5**, in both cases, typical π – π interactions were not detected, presumably owing to the nonplanar conformations of the phenothiazine units (Figure 10b, d). As is often observed with TADF-active materials, the Φ_{PL} value of the solid samples decreased as the atmosphere was changed from argon to air (e.g., from 0.93 to 0.66 for compound **4**). Intriguingly, D–A–D' compound **4** not only exhibited AIDF characteristics, but also mechanoluminescence (ML),^[78] which is luminescence that is induced by a mechanical stimulus, such as grinding, rubbing, cutting, and scratching. Similar symmetrical AIDF-active D–A–D triads (D = phenoxazine or phenothiazine, A = diphenylsulfone or dibenzothiophene-*S,S*-dioxide) were also reported by Zhao, Tang, and co-workers in 2015.^[79]

The most promising application of AIDF-active emitters is as a non-doped emitting layer in OLEDs, as mentioned above, and several groups have developed AIDF-active compounds and applied them in non-doped OLED devices. The Lee group synthesized asymmetric D–A–D' emitter **PTSOP** (Figure 11), which exhibited a small ΔE_{ST} value of 90 meV in toluene, and employed it in non-doped OLED devices.^[80] According to theoretical calculations, the molecule adopted an almost-orthogonal D–A structure (98° and 103°) in the gas phase (Figure 11), which can prevent intermolecular electronic interactions to cause aggregation-caused quenching (ACQ) of the emission in

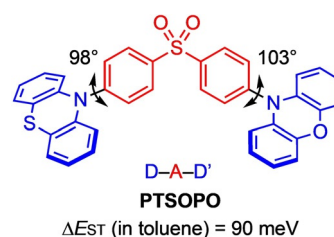


Figure 11. Molecular structure of **PTSOP**.

the condensed state. The OLED device that was fabricated with the configuration ITO/PEDOT:PSS/TAPC/mCP/emitter/TSP01/TPBi/LiF/Al (PSS = poly(styrene sulfonate), TSP01 = diphenyl-4-triphenylsilylphenyl-phosphineoxide, TPBi = 1,3,5-tris(1-phenyl-1*H*-benzimidazol-2-yl)benzene) achieved a maximum EQE of 17.0%, which was comparable to that (17.7%) of a doped device that used DPEPO as the host matrix.

In 2016, Yasuda and co-workers developed unique Janus-type D–A–A' compounds that contained an *o*-carborane ($C_2B_{10}H_{12}$) as a σ -electron-accepting core (Figure 12a).^[81] In this case, the *o*-carborane unit allowed for spatial separation of the D and A' units to exclusively locate the HOMOs and the LUMOs on the D and A' units, respectively (Figure 12b). Intriguingly, there was effective electronic conjugation between the D and A (*o*-carborane) units, which was evident from elongation of the C_1 – C_2 bond in the *o*-carborane cage of **PCZ-CB-TRZ** (1.714 Å) compared to that in unsubstituted *o*-carborane (1.629 Å). This distinct HOMO/LUMO separation in the unsymmetrical D–A–A' structures resulted in quite-narrow ΔE_{ST} values (3 meV for **PCZ-CB-TRZ**; 146 meV for **TPA-CB-TRZ**), whilst the symmetrical D–A–D compound^[82] exhibited quite different

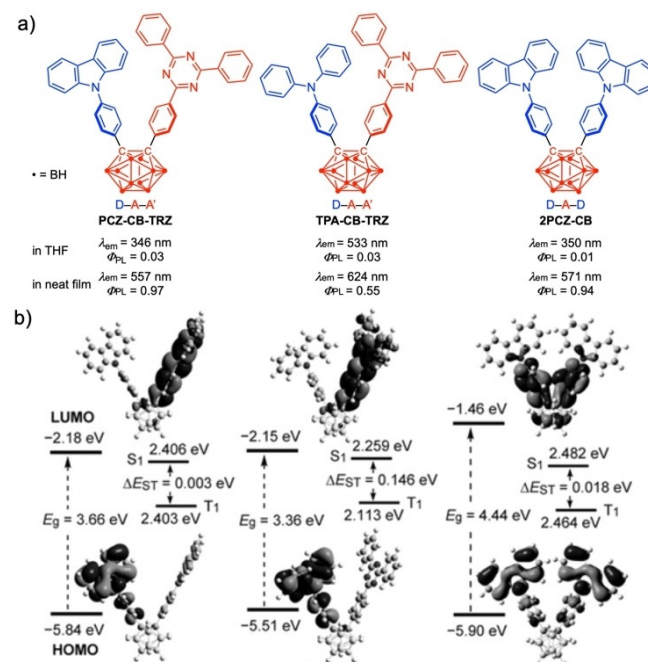


Figure 12. Molecular structures and photophysical data (a) and DFT calculations (b) of *ortho*-carborane-cored AIDF emitters. Adapted from Ref. [81].

frontier orbital distributions, yet with a rather small ΔE_{ST} value (18 meV; Figure 12b). The AIE character was evident from a comparison of the Φ_{PL} value in THF solution with those of the neat films. Non-doped OLED devices that were fabricated with the configuration ITO/ α -NPD/mCP/emitter/PPT/LiF/Al (α -NPD = *N,N'*-di(1-naphthyl)-*N,N'*-diphenyl-(1,1'-biphenyl)-4,4'-diamine, PPT = 2,8-bis(diphenylphosphoryl)dibenzo[*b,d*]thiophene) nicely showed yellow (λ_{em} = 586 nm with **PCZ-CB-TR**; λ_{em} = 590 nm with **2PCZ-CB**) and red (λ_{em} = 631 nm with **TPA-CB-TRZ**) EL with moderate EQEs (9.2–11.0%).

More recently, Lee, Lee, and co-workers developed unique AIDF-active zwitterionic D–A compounds by employing 7,8-dicarbo-*nido*-undecaborane ([C₂B₉H₁₀][−]), which is an anionic and open-cage analogue of *closo*-carboranes, as the donor and triarylborane as the acceptor (Figure 13a).^[83] These compounds were readily synthesized by deboration of the corresponding *closo*-carborane–triarylborane diads by using tetrabutyl ammonium fluoride (TBAF). The absorption spectra of dilute solutions of *nido*-**mn** (*n* = 1–4) in THF showed a strong absorption at $\lambda \approx 310$ nm, which is typical of the π (Mes) → p_π (B) CT transition, along with a weak absorption at $\lambda \approx 350$ nm, which was ascribed to an ICT transition from the *nido*-carborane (D) to the PhBMe₂ moiety (A). Slight red-shifts of the absorption spectra of solutions of *nido*-**pn** (*n* = 1–4) in THF from those of *nido*-**mn** indicated increased electronic interactions between the HOMOs and LUMOs of the *nido*-**pn** compounds. Significant AIE characteristics of *nido*-**m2** and *nido*-**m3** were evident from the

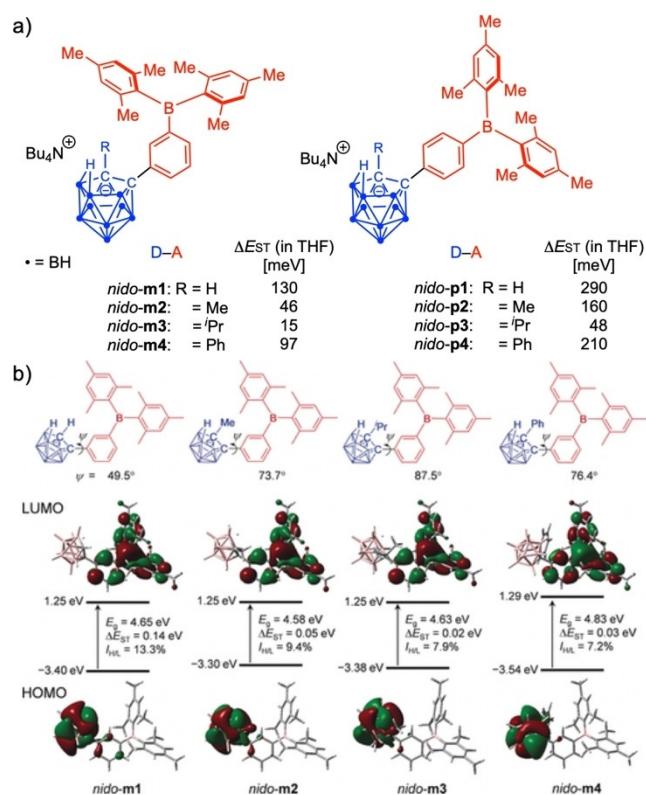


Figure 13. a) Molecular structures of *nido*-**m1**–*nido*-**m4** and *nido*-**p1**–*nido*-**p4**; b) DFT calculations of *nido*-**m1**–*nido*-**m4**. Adapted from Ref. [83]. $I_{H/L}$ = the overlap integral extents between the HOMO and the LUMO.

higher Φ_{PL} values in the PMMA films (0.35 and 0.33) compared with those in THF (0.03 and 0.04, respectively). This AIE effect was probably owing to significant steric hindrance of the *nido*-carborane units to suppress intermolecular electronic interactions in the solid state. Transient PL decay of the CT emission of *nido*-**mn** as solutions in oxygen-free THF indicated the presence of two components: short-lived (τ_p = 17–44.9 ns) and long-lived (τ_d = 0.33–1.46 μ s) emissive species. In contrast, only *nido*-**p3** showed two components (τ_p = 25.8 ns; τ_d = 0.41 μ s) among the *para*-substituted derivatives, thus indicating that the substitution pattern (*meta* or *para*) and the steric hindrance of the R group influenced the AIDF properties. DFT calculations suggested that the larger steric bulk of the R group induces twisting of the phenylene against the plane that included the dicarbon units of the carborane donor (Figure 13b), thereby resulting in separation of the HOMO and LUMO and a narrow ΔE_{ST} .

Yasuda and co-workers synthesized AIDF-active D–A compounds **PTZ-XT** and **PTZ-BP** (Figure 14a).^[84] Neat films of both compounds showed yellow emissions (λ_{em} = 545 nm for **PTZ-XT**; λ_{em} = 565 nm for **PTZ-BP**) with good Φ_{PL} values (0.53 and 0.31 under a N₂ atmosphere, respectively), as well as narrow ΔE_{ST} values (71 nm and 65 nm, respectively). An AIE test with THF/water mixtures clearly revealed AIE behavior, with a dramatic increase in PL intensity upon the formation of aggregates at water fractions (f_w) higher than 80–85% (Figure 14b,c). TADF characteristics of both compounds were supported by the narrow ΔE_{ST} values, the presence of two emissive components on the nanosecond and microsecond timescales, and air-sensitive Φ_{PL} values. Non-doped OLED devices with the configuration ITO/ α -NPD/mCBP/emitter/B3PyPB/Liq/Al exhibit yellow EL (λ_{em} = 553 nm for the device with **PTZ-XT**; λ_{em} = 577 nm with **PTZ-BP**; mCBP = 3,3'-di(9H-carbazol-9-yl)-1,1'-biphenyl, B3PyPB = 1,3-bis(3,5-dipyrid-3-ylphenyl)benzene, Liq = 8-hy-

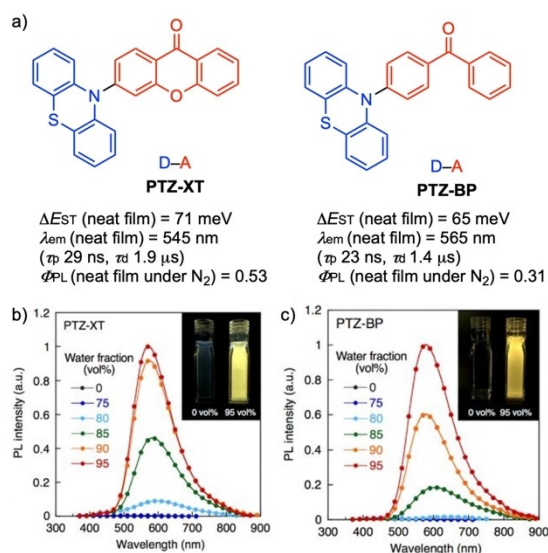


Figure 14. a) Molecular structures and photophysical data of **PTZ-XT** and **PTZ-BP**. b, c) Plot of the PL intensities of **PTZ-XT** (b) and **PTZ-BP** (c) as a function of water fraction (f_w) in THF/water mixtures. Adapted with permission from Ref. [84]. Copyright 2016, Springer Nature.

droxyquinolinato lithium), with maximum EQEs of 11.1 and 7.6%, respectively.

D–A-type dendritic organic emissive compounds are promising AIDF-active and solution-processable emitters, because dendritic molecular architectures can suppress intermolecular interactions, thereby enhancing solubility in organic solvents. In 2016, Jiang, Sun, and co-workers developed D–A compounds **tCzDSO2** and **3tCzDSO2**, which comprised thianthrene tetraoxide (A) and carbazole or carbazolyl dendrons (D; Figure 15a).^[85] The dendritic structures resulted in higher thermal

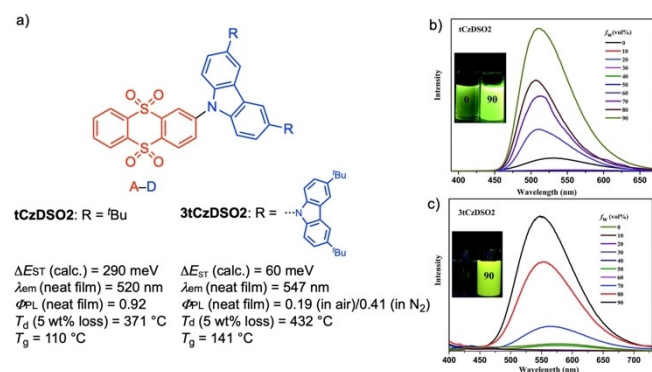


Figure 15. a) Molecular structures and physicochemical data of **tCzDSO2** and **3tCzDSO2**. b, c) Plot of the PL intensities of **tCzDSO2** (b) and **3tCzDSO2** (c) as a function of water fraction (f_w) in THF/water mixtures. Adapted with permission from Ref. [85]. Copyright 2016, Royal Society of Chemistry.

stability compared to small molecules (e.g., $T_d = 432$ °C for **3tCzDSO2**; $T_d = 371$ °C for **tCzDSO2**), owing to the increased molecular weight. Such a feature is advantageous for fabricating OLED devices. An AIE test in THF/water mixtures indicated that the emitters started to aggregate at $f_w = 60\%$ for **tCzDSO2** and at $f_w = 70\%$ for **3tCzDSO2**, as evident from a significant enhancement in the emission intensities (Figure 15b,c). Whilst the transient PL decay of the solid of **tCzDSO2** only showed a single component with a short lifetime ($\tau_p = 16$ ns), **3tCzDSO2** showed a two-component decay with short ($\tau_p = 29$ ns) and longer lifetimes ($\tau_d = 1.6$ μ s). The delayed component of **3tCzDSO2** also showed positive temperature dependence, in good agreement with typical TADF behavior, which was suggestive of distinct HOMO/LUMO separation as induced by the twisted dendritic structure.

Yamamoto and co-workers developed D–A–D-type dendrimers **G2B** and **G3B**, which were comprised of a benzophenone acceptor and carbazolyl dendrons as donors (Figure 16a).^[86] Neat films of both dendrimers exhibited moderately narrow ΔE_{ST} values (120 and 100 meV, respectively), green TADF with a maximum at $\lambda_{em} \approx 500$ nm, and moderate Φ_{PL} values (0.33 and 0.21, respectively), which were higher than those in deoxygenated toluene solutions (0.23 and 0.14, respectively). The Φ_{TADF} values of neat films of **G2B** (0.134) and **G3B** (0.136) were much higher than that of **G1B** (0.00004), thus highlighting the merit of the dendritic structure to afford efficient AIDF characteristics over small-molecular-weight derivatives in the aggregate state. In an AIE test with the PMMA matrix, the Φ_{PL} values of **G2B**

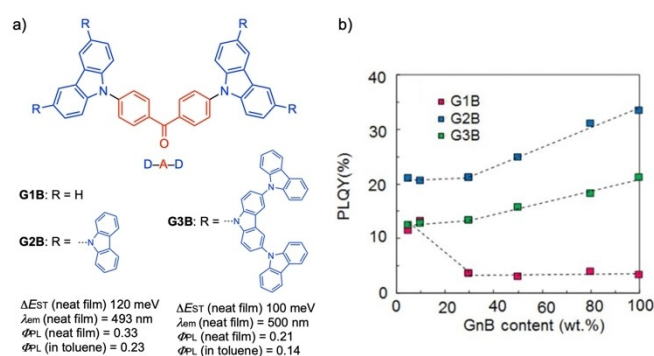


Figure 16. a) Molecular structures and photophysical data of **GnB** ($n = 1–3$). b) Plot of the PLQY values of **GnB** ($n = 1–3$) as a function of emitter content in a PMMA matrix. Adapted with permission from Ref. [86]. Copyright 2016, Springer Nature. PLQY = photoluminescence quantum yield, PMMA = poly(methyl methacrylate).

and **G3B** increased as the emitter content increased, which was the opposite behavior to that of small molecule **G1B** (Figure 16b). Solution-processed and non-doped OLED devices based on the structure ITO/PEDOT:PSS/PVK/emitter/TPBi/Ca/Al (PVK = poly(9-vinylcarbazole)) were fabricated by spin-coating the dendrimers to form non-doped EMLs. The OLEDs exhibited green EL, with maximum EQEs of 5.7% (for the device with **G2B**) and 3.6% (with **G3B**), which were much higher than those with a doped emitting layer in mCP host material ($EQE_{max} \approx 1.2\%$ for **G2B**; $EQE_{max} \approx 0.8\%$ for **G3B**).

Zhao, Su, Tang, and co-workers developed a series of AIDF-active D–A–D' compounds: **DBT-BZ-DMAC**,^[87] **DBT-BZ-PXZ**, and **DBT-BZ-PTZ** (Figure 17a).^[88] In the single-crystal structures of **DBT-BZ-DMAC** and **DBT-BZ-PXZ**, the donor units were highly twisted against the benzoyl accepting units (87° for **DBT-BZ-DMAC**, 66° for **DBT-BZ-PXZ**; Figure 17b,c). Whilst C–H $\cdots\pi$ and $\pi\cdots\pi$ interactions between bimolecular units were observed in **DBT-BZ-DMAC** (Figure 17d), multiple C–H $\cdots\pi$ and C=O \cdots H interactions (2.99–3.13 Å) were found in **DBT-BZ-PXZ** (Figure 17e). These noncovalent interactions “locked” the molecules to each other, thereby suppressing molecular motions that could dissipate the excitation energy. Intriguingly, **DBT-BZ-DMAC** showed bluish-green mechanoluminescence (ML)^[78] upon scratching of the crystalline powder. PL spectra of neat films of all of the compounds exhibited a significant blue-shift, presumably owing to the twisted conformations in the aggregated state. In this regard, the Φ_{PL} values of the neat films were much higher than those of the THF solutions (Figure 17a), in which more-planar structures with extended π -conjugated systems would be more favorable. Non-doped OLED emitters that employed D–A–D' compounds as the emitting layer with the configuration ITO/TAPC/emitter/TmPyPB/LiF/Al achieved good-to-high EQEs (14.2% for the device with **DBT-BZ-DMAC**, 9.2% with **DBT-BZ-PXZ**, and 9.7% with **DBT-BZ-PTZ**), with low turn-on voltages (ca. 2.7 V) and low-efficiency roll-off character (e.g., the roll-off of current efficiencies at 1000 cd m^{-2} were 0.46% with **DBT-BZ-DMAC**, 26.1% with **DBT-BZ-PXZ**, and 12.4% with **DBT-BZ-PTZ**). A subsequent theoretical investigation by Lin, Wang, and co-workers suggested that

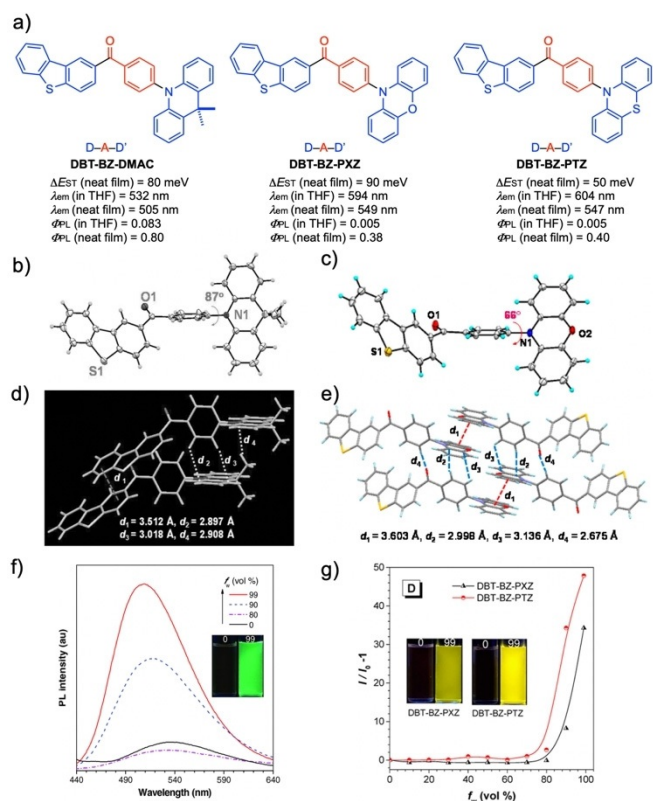


Figure 17. a) Molecular structures and photophysical data of DBT-BZ-DMAC, DBT-BZ-PXZ, and DBT-BZ-PTZ. b–e) Molecular geometries (b, c) and packing structures (d, e) of DBT-BZ-DMAC and DBT-BZ-PXZ, respectively, as determined by using X-ray crystallography. f, g) Plots of the PL intensity of DBT-BZ-DMAC (f) and the change in PL intensities of DBT-BZ-PXZ and DBT-BZ-PTZ (g) as a function of water fraction in THF/water mixtures. Adapted with permission from Refs [87,88]. Copyright 2017, American Chemical Society for Ref. [88].

the AIE character of DBT-BZ-PXZ was induced by restriction of the nonradiative decay caused by an intramolecular twisting motion between the carbonyl and phenylene plane and the C=O stretching modes.^[89] Furthermore, their calculations indicated that the efficient TADF behavior of DBT-BZ-PXZ in the solid state was not only attributed to the smaller ΔE_{ST} value, but also to the larger SOC constants (0.700 cm^{-1}) than in the THF solutions.

A similar series of D–A–D' compounds have also shown promise as OLED emitters with low-efficiency roll-off (Figure 18).^[90] Non-doped OLED devices with the configuration ITO/TAPC/emitter/TmPyPB/LiF/Al showed green-to-yellow EL

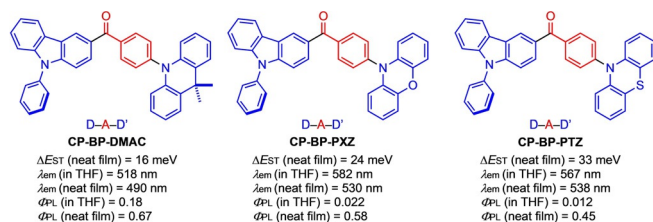


Figure 18. Molecular structures and photophysical data of CP-BP-DMAC, CP-BP-PXZ, and CP-BP-PTZ.

($\lambda_{em} = 502\text{--}554 \text{ nm}$), with low turn-on voltages (2.5–2.7 V) and high EQEs (15.0–18.4%). Most importantly, these devices showed very low current efficiency roll-off (0.2% for CP-BP-DMAC, 1.2% for CP-BP-PXZ, and 16.5% for CP-BP-PTZ at 1000 cd m^{-2}). In contrast, doped OLEDs that employed CBP as the host material showed significant roll-off (9.8–66.1%, depending on the doping amounts), thus showcasing the promise of AIDF-active compounds as low-roll-off OLED emitters. Single-carrier device measurements and cyclic voltammetry analysis suggested that the bipolar potential of the AIDF emitters facilitated balanced carrier injection and recombination to achieve high performance.

Ma, Yang, and co-workers developed efficient D–A- and D₃–A-type AIDF emitters by utilizing diphenylquinoxaline as a common acceptor and dimethyldihydroacridine (DMAC) and phenoxazine (PXZ) as donors (Figure 19a).^[91] All of the compounds showed AIE characteristics (Figure 19b–e), as well as typical TADF in degassed toluene solutions. The lifetimes of the delayed component for the DMAC-containing compounds ($\tau_d = 25.7 \mu\text{s}$ for SBDBQ-DMAC, $33 \mu\text{s}$ for DBQ-3DMAC) were approximately 10-times longer than those of the PXZ-containing compounds ($\tau_d = 2.86 \mu\text{s}$ for SBDBQ-PXZ, $1.38 \mu\text{s}$ for DBQ-3PXZ). Doped OLED devices that were fabricated with these emitters in the configuration ITO/MoO₃/TAPC/mCP/emitter in CBP (10 wt %)/Bphen/LiF/Al (Bphen = bathophenanthroline) ex-

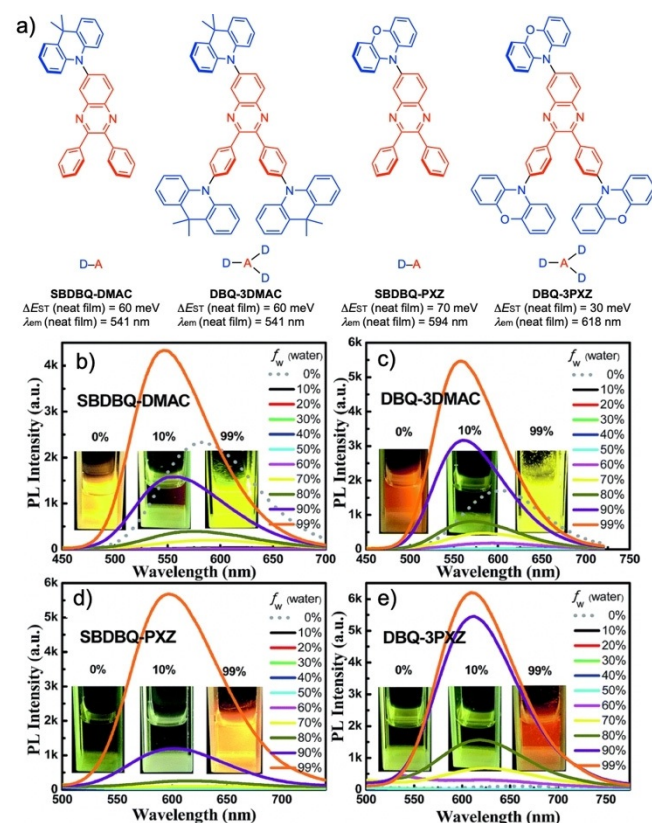


Figure 19. a) Molecular structures and photophysical data of SBDBQ-DMAC, DBQ-3DMAC, SBDBQ-PXZ, and DBQ-3PXZ. b–e) Plots of the PL intensities of SBDBQ-DMAC (b), DBQ-3DMAC (c), SBDBQ-PXZ (d), and DBQ-3PXZ (e) as a function of water fraction in THF/water mixtures. Adapted with permission from Ref. [91]. Copyright 2017, Royal Society of Chemistry.

hibited green (with DMAC-containing emitters) and orange (with PXZ-containing emitters) EL with high EQEs (11.1–22.4%) and low roll-offs. Of the OLEDs based on these D–A and D₃–A emitters, the devices that employed compounds with more D units (D₃–A-type compounds) showed better performance in terms of roll-offs and EQEs. Furthermore, by making use of their AIDF feature, non-doped OLEDs with a similar device structure achieved moderate EQEs (5.3–12.0%).

Similar D–A–D compounds **SFDBQPXZ** and **DFDBZPXZ** also showed nice TADF and AIE properties (Figure 20).^[92] As designed, both compounds showed small ΔE_{ST} values (ca. 40 meV) in the neat films. The presence of multiple noncovalent interactions, such as C–H...N, C–H...F, and C–H... π interac-

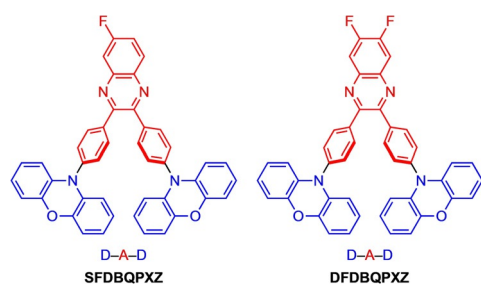


Figure 20. Molecular structures of **SFDBQPXZ** and **DFDBZPXZ**.

tions, were observed in the crystal structures of these compounds, thus implying that these interactions restricted the molecular motion in the solid state to suppress non-irradiative energy dissipation of the excitons. Vacuum-deposited OLEDs with the configuration ITO/MoO₃/TAPC/emitter in CBP (10 wt%)/Bphen/LiF/Al showed yellow EL (λ_{em} = 548 nm) with high maximum EQEs of up to 23.5% when **SFDBQPXZ** was used as an emitter. Devices that employed a non-doped emitting layer showed slightly red-shifted EL (λ_{em} \approx 580 nm) and moderate EQEs (10.1% for **SFDBQPXZ**; 9.8% for **DFDBQPXZ**). Notably, a non-doped OLED device with an unfluorinated derivative as an emitter (i.e., phenoxazine–phenylene–quinoxaline–phenylene–phenoxazine) with the same device configuration showed a lower EQE value (8.8%) than devices with fluorinated emitters, thus suggesting that fluorine played an important role in enhancing the OLED performance.

Chen, Shi, Tang, and co-workers developed a multidonor-substituted benzophenone (D₂–A–D') as an AIDF-active compound (**DCPDAPM**; Figure 21 a).^[93] In THF/water mixtures, the compound started to form aggregates at $f_w > 80\%$. The Φ_{PL} value dramatically increases from 6.2% in dilute THF solution ($f_w = 0\%$) to 76.1% ($f_w = 95\%$), with an increase in PL intensity (Figure 21 b). A non-doped OLED device with the configuration ITO/HATCN/TAPC/emitter/TmPyPB/LiF/Al (HATCN = 1,4,5,8,9,11-hexaazatriphenylene-hexacarbonitrile) showed a moderate EQE of 8.15% with a low turn-on voltage (3.2 V). The current efficiency roll-off at 1000 cd m⁻² was moderately low (20.4%). The authors also fabricated doped OLED devices by using CBP as a host material (20 wt% emitter), which showed a high EQE of 19.6%.

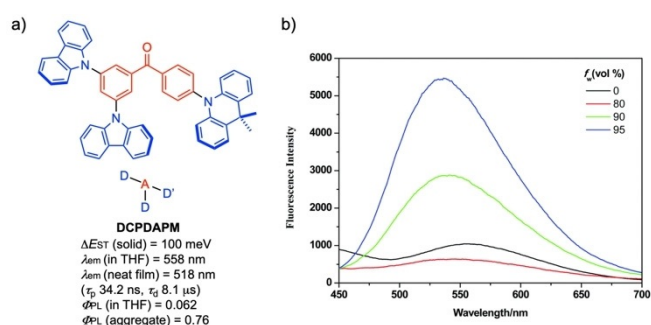


Figure 21. a) Molecular structure and photophysical data of **DCPDAPM**. b) Plots of the PL intensity of **DCPDAPM** as a function of water fraction in THF/water mixtures. Adapted with permission from Ref. [93]. Copyright 2018, Royal Society of Chemistry.

More recently, Wang and co-workers synthesized a D–A compound that comprised phenoxazine (D) and *N*-phenylphenothiazine dioxide (A) units (**PXZ2PTO**; Figure 22 a).^[94] In the single crystal, each molecule interacted with its neighboring molecules through face-to-face π – π , C–H... π , and C–H...O interactions (Figure 22 b). An AIE test in THF/water mixtures showed that aggregation began at $f_w > 70\%$. A non-doped OLED device with the structure ITO/MoO₃/TAPC/mCP/emitter/DPEPO/TPBi/LiF/Al showed green EL (λ_{em} = 504 nm), with a high maximum EQE (16.4%) and low-efficiency roll-off (EQE = 15.1% at 1000 cd m⁻²), which was comparable to those of the doped OLEDs.

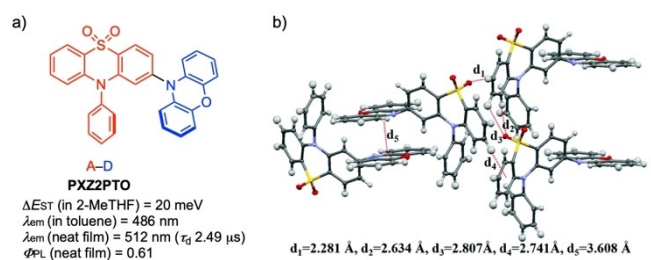


Figure 22. a) Molecular structure and photophysical data of **PXZ2PTO**. b) Packing structure of **PXZ2PTO** in the single crystals. Adapted with permission from Ref. [94]. Copyright 2018, Royal Society of Chemistry.

4.2. TADF-Active and Mechanochromic Luminescent (MCL) Materials

Mechanochromic luminescent (MCL) materials can reversibly change emission color when an external stimulus, such as a mechanical force (e.g., grinding, pressing, rubbing, and shearing), temperature, organic vapor, or an electric field, is applied.^[95] Because of their unique features, MCL-active materials have a range of applications, such as security inks, nondestructive pressure sensors, temperature sensors, and molecular encryption. Over the last decade, significant advancements have been made in MCL-active organic materials.^[95] It would be reasonable to think that combining MCL and TADF functions into a single molecule would offer us opportunities to develop multifunctional emissive organic materials beyond the convention-

al emitters. However, despite the potential utility of TADF-active MCL materials, research into such organic materials remains in its infancy. In this section, TADF-active materials that show mechano-induced luminescence^[96] or MCL changes are categorized into three subgroups: 1) white-light-emitting (dual-emitting) systems; 2) bicolor-changing systems; and 3) multicolor-changing systems.

4.2.1. TADF-Active White-Light-Emitting (Dual-Emitting) Materials that Exhibit Mechano-Induced Luminescence Changes

TADF-active white-light-emitting materials based on a single component hold great promise for lighting applications. To realize white emission with a single component, the materials are required to emit dual emission in the blue and orange regions. In addition to their dual-emitting characteristics, tunability of the Commission Internationale de l'Éclairage (CIE) coordinates by using an external stimulus would offer the ability to adjust color tones without changing the material's compositions. In 2015, Zhang, Chi, Bryce, and co-workers developed single-molecular white-emitting compounds **OPC**^[97] and **SCP**^[98] which had an unsymmetrical D–A–D' structure (Figure 23a). The white PL (CIE coordinates of the powder: 0.35, 0.35) of **OPC** consisted of a dual emission (blue fluorescence and yellow CT-emission TADF), presumably owing to a mixture of two different CT emissions from different conformers ("quasi-axial" and "quasi-equatorial").^[99] **OPC** also showed typical AIE behavior (i.e., **OPC** was AIDF-active). The TADF behavior of **OPC** in the solid state was confirmed by the long-lived emission components in the transient PL decay, the temperature-dependent emissions, and the oxygen-sensitive Φ_{PL} value. Notably, the emission color of **OPC** was sensitive to temperature and grinding. A mechano-induced ratiometric change in emission color was achieved by grinding the white-emissive crystalline

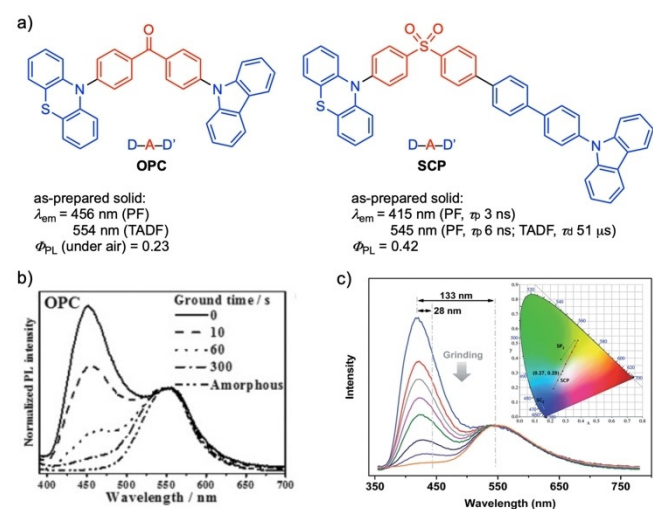


Figure 23. a) Molecular structures and photophysical data of **OPC** and **SCP**. b, c) Mechano-induced PL spectra of **OPC** (b) and **SCP** (c) in the single crystals. Adapted with permission from Ref. [97,98]. Copyright 2016, Royal Society of Chemistry for Ref. [98]. $\text{SC}_2 = 9,9'$ -(sulfonylbis(1,1'-biphenyl)-4',4'-diyl)bis(9*H*-carbazole), $\text{SP}_2 = 10,10'$ -(sulfonylbis(4,1-phenylene))bis(10*H*-phenothiazine).

sample of **OPC**, thereby gradually leading to a yellow-emissive amorphous sample (Figure 23b). Alongside the change in emission color, the intensity of the normal fluorescence at $\lambda_{\text{em}} = 456$ nm decreased as a mechanical force was applied, whilst that of the delayed emission at $\lambda_{\text{em}} = 554$ nm remained intact (Figure 23b). A similar mechano-induced luminescence change was also observed with another D–A–D' compound, **SCP**, which showed a decrease in the intensity of the blue normal fluorescence ($\lambda_{\text{em}} = 415$ nm, $\tau_{\text{p}} = 3$ ns) and unchanged yellow TADF ($\lambda_{\text{em}} = 545$ nm, $\tau_{\text{d}} = 51$ μs) as a mechanical force was applied (Figure 23c). The authors suggested that this mechano-induced gradual luminescence change of **SCP** (from "ON–ON" to "OFF–ON") was correlated to a change in the local conformations of the molecule (e.g., planarization of the phenylcarbazole unit).

In 2018, Li and co-workers reported that a mechanoluminescence (ML)-active D–A compound, **FCO-CzS**, showed a similar mechano-induced ratiometric emission-color change (Figure 24a).^[100] Upon grinding crystals of **PCO-CzS**, the emission

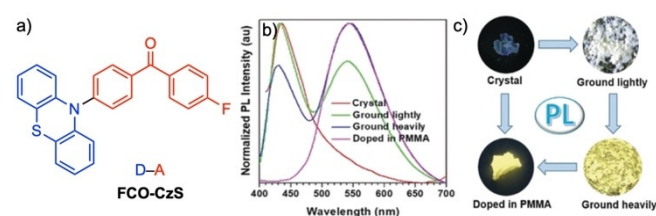


Figure 24. a) Molecular structure of **FCO-CzS**. b) PL spectra of **FCO-CzS** in different morphologies. c) Photographs of **FCO-CzS** in different solid states under UV irradiation ($\lambda = 365$ nm). Adapted from Ref. [100].

color changed from blue ($\lambda_{\text{em}} = 434$ nm, prompt fluorescence) to light yellow ($\lambda_{\text{em}} = 434$ and 544 nm, prompt fluorescence and delayed fluorescence; Figure 24b). The authors ascribed this dramatic change in emission profile to variation in the irradiative pathway (PF to delayed fluorescence) as induced by a conformational change in the phenothiazine unit. This result was reasonably explained by the much lower calculated ΔE_{ST} value for the quasi-equatorial conformer (10 meV) compared to that of the quasi-axial conformer (720 meV), thus indicating that the conformation with a narrower ΔE_{ST} value would facilitate rISC from the T_1 to S_1 states to yield TADF.

As mentioned above (Section 3), Bryce and co-workers elegantly revealed that D–A compound **OPM** (Figure 25a), which adopted a quasi-axial conformation in the single-crystal state, emitted RTP (Figure 25b), whereas its regioisomer **OMP** (Figure 25a), which adopted a quasi-equatorial conformation, exclusively irradiated TADF (Figure 25c).^[72] Given this report, it was speculated that the observation of a mechano-induced emission-color change in **FCO-CzS**, as disclosed by the Li group,^[100] could correspond to an emission change from RTP to TADF as a result of a conformational change from quasi-axial to quasi-equatorial.

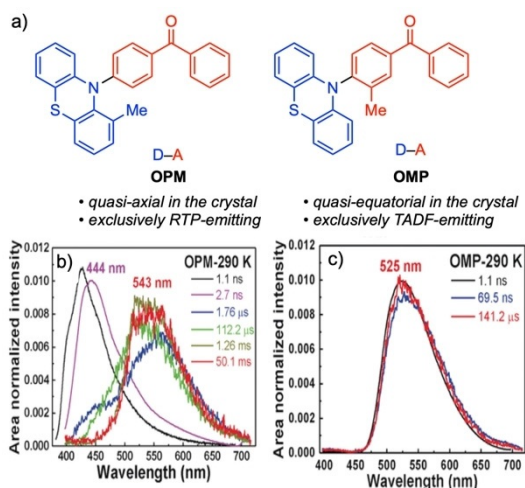


Figure 25. a) Molecular structures of OPM and OMP. b, c) Time-resolved normalized PL spectra of crystals of OPM (b) and OMP (c) at 290 K. Adapted from Ref. [72].

4.2.2. TADF-Active Materials that Exhibit Mechano-Induced Emission-Color Changes or Mechanochromic Luminescence in a Bicolor System

Chi, Chou, and co-workers developed a series of twisted D–A compounds in which dimethylacridine was employed as the donor and pyrimidine was employed as the acceptor (T1–T4; Figure 26a).^[101] X-ray crystallographic analysis revealed highly twisted structures of T1 and T2 around the D–A connecting bond (88.76° for T1; 85.49° for T2), which caused distinct separations of the HOMOs and LUMOs to decrease the ΔE_{ST} value. These compounds showed typical CT-type TADF properties, both in solution and in the solid state. By comparing their solvatochromic behavior, ΔE_{ST} values, and the energy gaps in T1–T4, the authors concluded that the CT ability of this series of compounds followed the order T2 > T4 > T1 > T3. Compound T2 exhibited a significant mechano-induced emission-color change (Figure 26b). Blue emission ($\lambda_{em} = 433$ nm) in the single

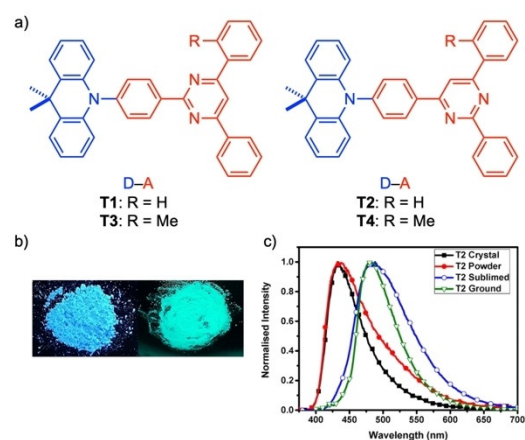


Figure 26. a) Molecular structures of T1–T4. b) Luminescence of T2 before (left) and after (right) mechanical grinding. c) PL spectra of T2 in different morphologies. Adapted from Ref. [101].

crystals underwent a red-shift to cyan ($\lambda_{em} = 483$ nm) and green ($\lambda_{em} = 490$ nm) upon grinding with a pestle and mortar and sublimation, respectively (Figure 26c). To revert back to the original blue-light-emitting state, recrystallization of the cyan- and green-emissive solids from organic solvents was required. Based on crystallographic analysis, it was proposed that breaking up the H-aggregates, which were held together by π - π interactions, by using mechanical force or sublimation resulted in looser packing structures, which led to red-shifted emissions. OLED devices with the configuration ITO/TAPC/emitter in mCP (10 wt%)/emitter in DPEPO in mCP (10 wt%)/TmPyPB/LiF/Al showed blue EL ($\lambda_{em} = 472$ –492 nm) with moderate-to-good EQEs (7.2–14.2%), thus indicating that the rISC process smoothly proceeded in the emitting layer to induce TADF, even in the devices.

In 2017, Baldo, Swager, and co-workers developed unique TADF materials based on a donor–bridge–acceptor (D–b–A) scaffold by using xanthene as a bridging spacer unit (Figure 27a).^[102] Through-space intramolecular CT allowed for the realization of a small ΔE_{ST} value (< 10 meV based on DFT calculations), whilst a perpendicular molecular geometry with restricted molecular motion led to AIDF. These materials were readily synthesized through successive Ullman-type amination (to install the D unit) and palladium-catalyzed arylation (to install the A unit) reactions of 4,5-diiodo-9,9-dimethylxanthene. X-ray crystallographic analysis revealed that the D and A moieties were aligned almost parallel to one another and the interchromophore distances (i.e., the distance between the π -planes of the D and A units; 3.29–3.42 Å), which were shorter

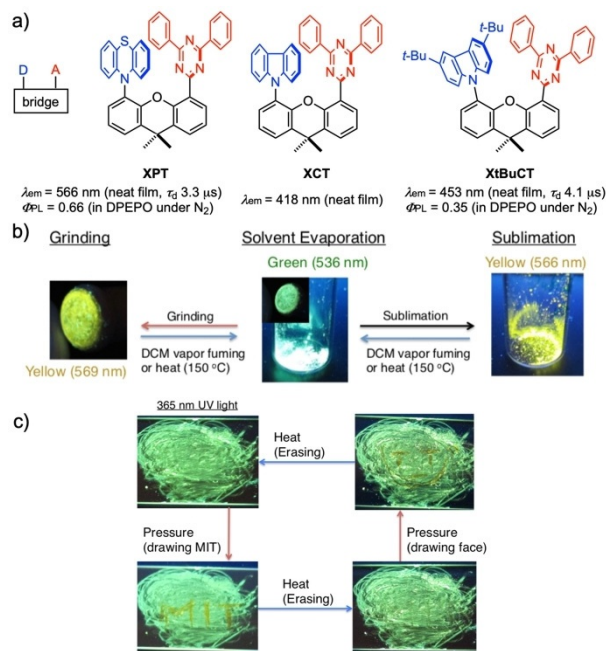


Figure 27. a) Molecular structures and photophysical data of XPT, XCT, and XtBuCT. b) Changes in the luminescence of XPT in response to grinding, sublimation, and vapor fuming. c) Writing and erasing of a luminescent encryption on a glass substrate by using XPT. Adapted with permission from Ref. [102]. Copyright 2017, American Chemical Society. DPEPO = bis[2-[(oxo)diphenylphosphino]phenyl] ether.

than calculated values (3.8–4.5 Å), were suitable for through-space interactions. As expected, the emission properties of these D–A compounds were sensitive to the presence of molecular oxygen. In addition, these compounds were AIE-active, as evident from a dramatic increase in the emission intensity as the f_w increased in THF/water mixtures. This change, which would be caused by restriction of the molecular rotation, was supported by X-ray crystallographic analysis, in which intermolecular C–H... π interactions seemed to be present. Among these AIDF-active compounds, **XPT** showed noticeable bicolor-changing MCL behavior. Crystals that were grown by evaporation from pentane emitted bright-green light ($\lambda_{em} = 536$ nm). Then, upon grinding with a pestle and mortar, the solid sample exhibited yellow PL ($\lambda_{em} = 569$ nm; Figure 27 b). In this case, the green-emitting state was nicely recovered by fuming with CH_2Cl_2 vapor or by heating above the glass transition temperature (Figure 27 b). By making use of the reversibility of these green–yellow emission states by using external stimuli, the authors demonstrated the writing and erasing of a fluorescent encryption on a glass substrate (Figure 27 c). Furthermore, OLEDs devices that were fabricated by using **XPT** and **XtBuCT** with the configuration ITO/TAPC/emitter in DPEPO (10 wt%)/DPEPO/TmPyPb/LiF/Al showed EL peaks at $\lambda = 584$ and 488 nm, respectively, with moderate EQEs (e.g., 10% with the **XPT** emitter).

Sun, Jiang, and co-workers reported that an AIE-active^[103] TADF D–A compound, **Cz-AQ**, showed bicolor-changing MCL between yellow ($\lambda_{em} = 541$ nm) and red ($\lambda_{em} = 604$ nm; Figure 28 a).^[104] Crystal that exhibited a red emission (R-crystal) underwent a phase transition upon heating at 169 °C for a short period of time (5 s) into a yellow-emitting crystalline state (Y-crystal), whilst the reverse process (i.e., from Y-crystal to R-crystal) was readily implemented by fuming with CH_2Cl_2 vapor or by grinding (Figure 28 b). X-ray crystallographic analysis of the R- and Y-single crystals revealed small differences in the dihedral angles between the D and A units (R-crystal: 47.11°, Y-crystal: 48.08°). However, contrary to their geometrical similarities, the packing structures of these crystals were quite different: **Cz-AQ** formed J-type aggregates in the Y-crystal (Figure 28 c) but H-type aggregates in the R-crystal (Figure 28 d). The authors ascribed the MCL behavior of **Cz-AQ** to an alternation of

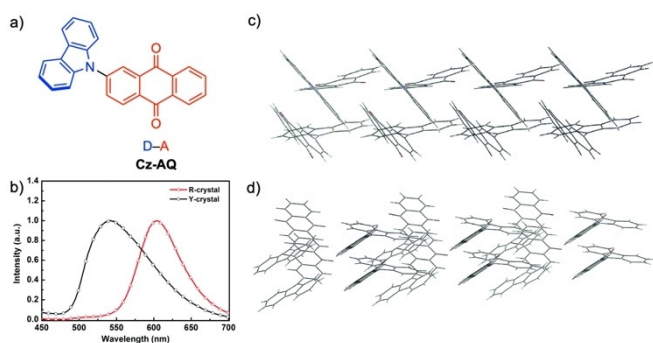


Figure 28. a) Molecular structure of **Cz-AQ**. b) PL spectra of R- and Y-crystals. c, d) Packing structures of Y-crystals (c) and R-crystals (d). Adapted with permission from Ref. [104]. Copyright 2017, Royal Society of Chemistry.

the packing modes. Intriguingly, non-doped OLED devices that were fabricated with the configuration ITO/PEDOT:PSS/emitter/TPBi/Cs₂CO₃/Al by using a solution process for the emitting layer (EML) nicely showed different EL spectra depending on the solvent that was used to deposit the EML. A device in which the EML was deposited from 1,2-dichloroethane showed a red EL, with a peak at $\lambda = 680$ nm, whilst a device in which the EML was deposited from a mixture of 1,2-dichloroethane and EtOH showed a blue-shifted EL peak at $\lambda = 600$ nm. However, disappointingly, the EQEs of these devices were very low (<1.5%), presumably owing to ACQ of the excitons in the condensed phase.

More recently, Lee and co-workers reported that a similar D–A compound, **PTZ-AQ**, which contained phenothiazine as a donor, showed multifunctional properties of AIDF, polymorphism, and a mechano-induced luminescence color change (Figure 29 a).^[105] Depending on the crystallization conditions, **PTZ-AQ** could adopt up to five different polymorphs with three different emission colors, yellow ($\lambda_{em} = 545, 554$ nm), orange ($\lambda_{em} = 568$ nm; O-crystal), and red ($\lambda_{em} = 606, 649$ nm), and various Φ_{PL} values within the range 0.02–0.84 (Figure 29 b). Among the different polymorphs, the R-crystal showed distinct TADF properties, with a very small ΔE_{ST} value (10 meV) and a high Φ_{PL} value (0.84). Based on X-ray crystallographic analysis, the molecule adopted almost the same conformation even in different polymorphs (Y-, O-, and R-crystals), but the packing structures were quite different (Figure 29 c–e). In the Y-crystal, two molecules formed parallel pairs through weak π – π -stacking interactions of the anthraquinone rings (ca. 40% overlap with a centroid–centroid distance of 3.66–3.76 Å; Figure 29 c), whereas, in the O-crystal, two molecules stacked in an antipar-

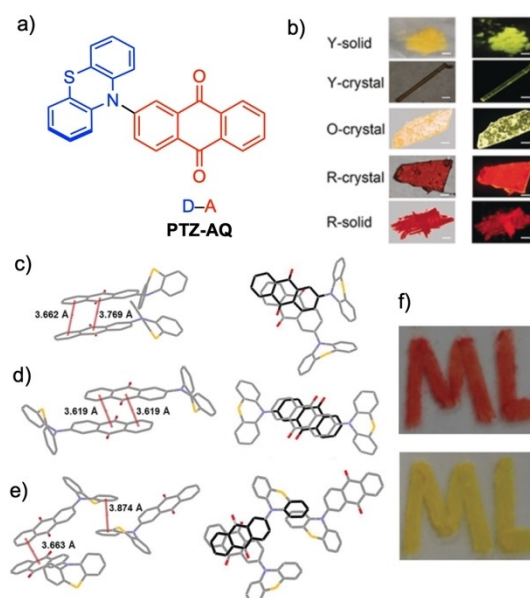


Figure 29. a) Molecular structure of **PTZ-AQ**. b) Photographs of polymorphs under ambient light (left) and under UV light (right). c–e) Packing structures of the Y-crystal (c), O-crystal (d), and R-crystal (e). f) Photographs of the R-solid in daylight (top) and after heating at 150 °C for 30 s in daylight (bottom). Adapted from Ref. [105].

allel manner with greater π - π overlap (67%) and a centroid-centroid distance of 3.61 Å (Figure 29d). Interestingly, in the R-crystal, three molecules aggregated through face-to-face stacking interactions at the anthraquinone (40% overlap) and phenothiazine (25% overlap of the benzene rings) moieties (Figure 29e). The authors suggested that this polymorphism-dependent emission was owing to a change in the degree of π - π interactions, as supported by DFT calculations. Furthermore, the R-solid of **PTZ-AQ** showed a mechano-induced luminescence color change upon heating at 150 °C for 30 seconds: the R-solid turned into the Y-solid state. Conversely, the Y-solid could be reversed back into the R-solid through evaporation of its solution in CH₂Cl₂ at room temperature (Figure 29f).

Su and co-workers reported a distinct bicolor emission change between blue and yellow with AIDF-active D-A compound **6** (Figure 30a),^[106] which had a similar molecular struc-

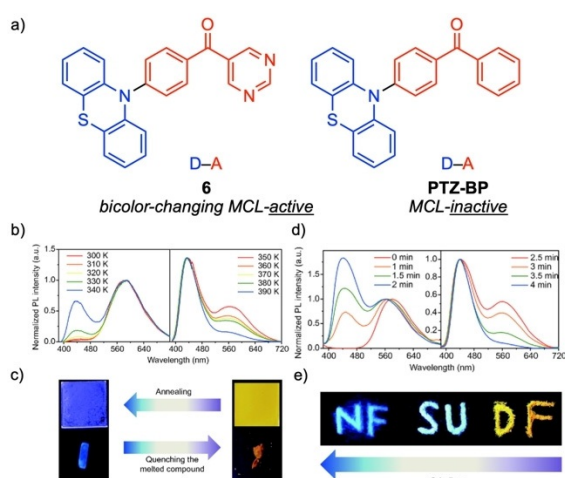


Figure 30. a) Molecular structures of compound **6** and PTZ-BP. b) Time-dependent PL spectra of a neat film of **6**. c) Photographs that show the MCL behavior of compound **6** as thin films and a single crystal under UV irradiation. d) PL spectra of a powdered sample of compound **6** as a function of grinding time. e) Photographs that show the MCL behavior of a powder of **6** on quenching/annealing. Adapted with permission from Ref. [106]. Copyright 2018, Springer Nature.

ture to emitter **PTZ-BP**.^[84] Thermal annealing of TADF-emitting neat films caused a gradual change in the EL spectrum from yellow (TADF) to deep blue (normal fluorescence) as the temperature increased (Figure 30b). Blue-emitting single crystals of compound **6** underwent a phase transition by thermal melting and subsequent solidification into yellow-emitting amorphous samples, which then reverted back into blue-emitting crystalline solids by grinding with a pestle and mortar (Figure 30c,d). In contrast, a similarly structured compound, **PTZ-BP**, did not exhibit such MCL behavior. Based on detailed photophysical inspection and theoretical calculations, the authors proposed a MCL mechanism that involved alternation of the conformations of the phenothiazine donor (quasi-axial and quasi-equatorial). Because a slight difference in the structure of the A unit (pyrimidine or benzene) brought about a big difference in the MCL behavior (MCL-active or MCL-inactive), pyrimidine should

play a significant role in switching the conformations in the ground and excited states.

4.2.3. TADF-Active Multicolor-Changing MCL Materials

The color-tunability of TADF-active MCL materials can offer significant opportunities for endowing organic emitters with additional value and, thus, possible applications such as multichannel sensing, color-tunable displays, and real-time image mapping. However, examples of multicolor-changing MCL materials themselves are sparse, presumably owing to the lack of general materials principles.^[95c] Only in the last few years have we witnessed the advancement of TADF-active multicolor-changing MCL materials, despite their promising applications.

The first examples of TADF-active multicolor-changing MCL materials were reported by Takeda, Data, and co-workers in 2017 (**7** and **8**; Figure 31 a).^[107] Their key concept for the material design was the use of conformationally switchable “flappy” electron donors in a TADF-active twisted D-A-D system,^[151] which employed a structurally and photophysically unique dibenzo[*a,j*]phenazine (DBPHZ)^[108] as an acceptor unit. Because phenothiazine (PTZ) can adopt two interconvertible conformers (quasi-axial, *ax*, and quasi-equatorial, *eq*; Figure 31 a), D-A-

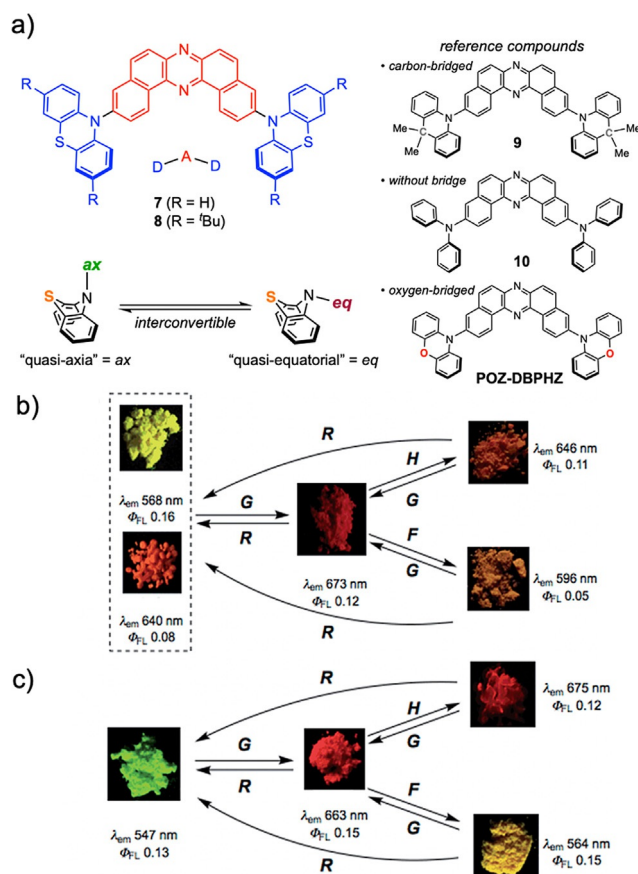


Figure 31. a) Molecular structures of D-A-D compounds **7**–**10**. MCL relationships and photographs of solid samples of compounds **7** (b) and **8** (c) under UV irradiation (R: recrystallization from *n*-hexane/CHCl₃, H: heating at 220 °C, G: grinding with a pestle and mortar, F: fuming with CH₂Cl₂ vapor). Adapted with permission from Ref. [107]. Copyright 2017, Royal Society of Chemistry.

D compounds **7** and **8** could each adopt four different conformers (*syn-ax-ax*, *anti-ax-ax*, *ax-eq*, and *eq-eq*) to show different emission colors. Both compounds exhibited distinct multicolor-changing MCL behavior in response to a variety of external stimuli, such as grinding, heating, and fuming (Figure 31 b,c). In sharp contrast, reference D–A–D compounds that contained donor units with a carbon bridge (**9**), without a bridge (**10**), and an oxygen bridge (POZ-DBPHZ)^[51] did not exhibit any significant change in emission color in response to similar stimuli (Figure 31 a). This result clearly indicated the importance of the sulfur atom in the D units for realizing multicolor-changing MCL properties. Taken together with their X-ray crystallographic analysis, the authors proposed a mechanism for the multicolor-changing MCL that involved alternation of the ICT character of the excited states, caused by the change in conformation (Figure 32). The emissive excited states of the

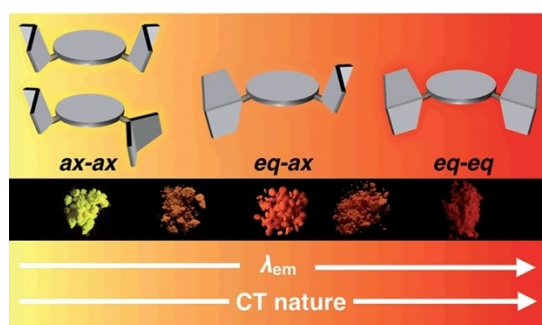


Figure 32. Proposed correlation between conformation and emission color. Adapted with permission from Ref. [107]. Copyright 2017, Royal Society of Chemistry.

ax-ax conformers of compounds **7** and **8** would have similar characteristics to the locally excited (LE) states of the A (DBPHZ) unit, whilst those of the highly twisted conformers (*eq-ax* and *eq-eq*) would be ICT excited states that were stabilized by the perpendicular structures, thereby resulting in the more-red-shifted emissions colors. In addition to their distinct MCL properties, these materials served as an efficient TADF emitter in OLEDs. An OLED device that was fabricated with the configuration ITO/NPD/emitter in CBP (10 wt%)/TPBi/LiF/Al by using compound **7** as the emitter exhibited orange EL ($\lambda_{em} = 613$ nm) with a high maximum EQE value of 16.8%.

Recently, Takeda, Data, and co-workers further reported a proof-of-concept paper by designing a D–A–D compound (**11**) that comprised dihydrophenosphanzine sulfide (DPPZS) units as donors and DBPHZ as an acceptor unit (Figure 33 a).^[109] Notably, this D–A–D compound nicely showed not only TADF- and tricolor-changing MCL properties, as expected, but also acid/base-responsive emission-color change, in which visible and near-infrared (NIR) emissions were reversibly switched (Figure 33 b). As evidence for their concept of conformation-dictated emission regulation, the single-crystal-to-single-crystal (SC-to-SC) transition that accompanied the conformational change from *eq-eq* to *ax-eq* brought about a significant change in emission color. Furthermore, the compound in Zeonex film showed dual emission of TADF and RTP, as a

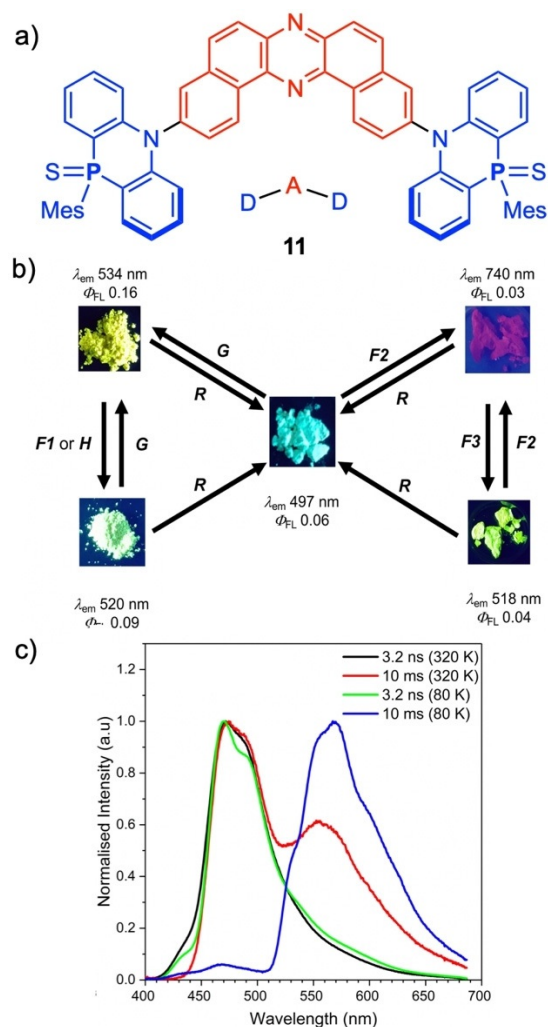


Figure 33. a) Molecular structure of D–A–D compound **11**. b) MCL relationships and photographs of solid samples of compound **11** under UV irradiation (R: recrystallization from *n*-hexane/CHCl₃, H: heating at 280 °C, G: grinding with a pestle and mortar, F1: fuming with CHCl₃ vapor, F2: fuming with trifluoroacetic acid vapor, F3: fuming with triethylamine vapor). c) PL spectra of compound **11** in a Zeonex film (1 wt%). Adapted with permission from Ref. [109]. Copyright 2018, Royal Society of Chemistry. Mes = mesityl.

consequence of a slower rISC process from the T₁ to S₁ states, hampered by a slightly larger ΔE_{ST} value (300 meV; Figure 33 c).

Dias, Grazulevicius, and co-workers developed a new series of TADF- and multicolor-changing MCL organic materials based on a D–A–D scaffold that comprised a quinoxaline as an acceptor unit and functionalized carbazoles as donors (Figure 34 a).^[110] Time-resolved spectroscopy revealed that the locally excited triplet state (³LE) of these D–A–D compounds gradually shifted to lower energy as the electron-donating ability of the installed donors increased in the order **CzQX** > **tCzQX** > **MeOQx** > **MeO2Qx**. This result indicated that, even in these highly twisted D–A systems, the donor and acceptor did not completely decouple, but still interacted with each other, depending on the electron-donating effect of the donor units. All of these materials showed alternating emission colors in the solid states upon the application of external stimuli, such

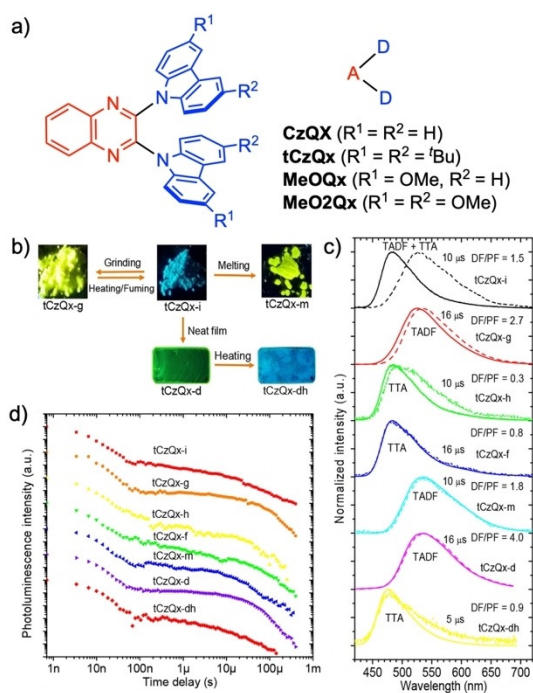


Figure 34. a) Molecular structures of **CzQx**, **tCzQx**, **MeOQx**, and **MeO2Qx**. b) MCL relationships and photographs of solid samples of **tCzQx** under UV irradiation. c, d) Time-resolved PL spectra (c) and PL-intensity decay (d) of different forms of **tCzQx**. Adapted with permission from Ref. [110]. Copyright 2018, American Chemical Society.

as grinding, heating, fuming, melting, and drop-casting (Figure 34b). In particular, **tCzQx**, **MeOQx**, and **MeO2Qx** exhibited a distinct color change from blue to red. Time-dissolved spectroscopic analysis revealed that TTA and TADF were switchable depending on the morphology of the compounds (Figure 34c,d). In the crystalline state, **tCzQx** showed a blue emission from the weak CT excited state (or hybrid local and CT state, HLCT), whilst the amorphous solid exhibited a red-shifted yellow color. The ΔE_{ST} value of the solid samples varied significantly from 160–420 meV, depending on their morphologies, owing to the dramatic change in the D–A dihedral angles. OLED devices that were fabricated with the emitters by using solution processes with the structure ITO/HIL/PVK/emitter in PVK:PBD (5 wt%)/TPBi/LiF/Al (HIL = hole-injection layer, PBD = 2-(4-*tert*-butylphenyl)-5-(4-biphenyl)-1,3,4-oxadiazole) showed moderate EQEs of up to 10.9%, thus suggesting that TADF was efficiently boosted in these devices.

Most recently, Yang and co-workers developed a series of TADF-active multicolor-changing MCL materials based on the D–A scaffold by using diphenyl [1,2,4]triazolo[1,5-*a*]pyrimidine (TzPm) as an acceptor and phenoxazine as a donor (Figure 35a).^[111] On doping in CBP matrix (0.7 wt% doping), all of the compounds showed typical TADF properties, with yellow emissions ($\lambda_{em} = 527\text{--}543$ nm, $\tau_d = 2\text{--}3$ μ s), narrow ΔE_{ST} values (60–100 meV), and good Φ_{PL} values (0.49–0.66, under an argon atmosphere). OLED devices that were fabricated by using solution processes based on the configuration ITO/PEDOT:PSS/emitter in CBP (0.7 wt%)/PmPyPB/Liq/Al showed yellow EL, with peaks within the range $\lambda = 542\text{--}560$ nm and good maxi-

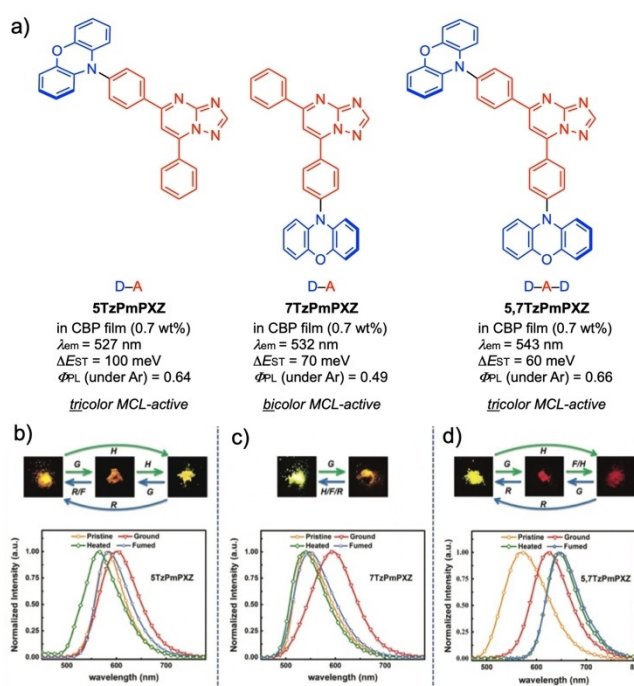


Figure 35. a) Molecular structures of **5TzPmPXZ**, **7TzPmPXZ**, and **5,7TzPmPXZ**. b–d) MCL relationships and photographs of solid samples of **5TzPmPXZ** (b), **7TzPmPXZ** (c), and **5,7TzPmPXZ** (d) under UV irradiation (R: recrystallization from *n*-hexane/ CHCl_3 , H: heating at 150 °C, G: grinding with a pestle and mortar, F: fuming with CH_2Cl_2 vapor). Adapted from Ref. [111].

mum EQEs of 9.3–14.3%. Interestingly, D–A compound **7TzPmPXZ** exhibited bicolor (yellow-orange) MCL behavior, whereas compounds that contained more donor units (**5TzPmPXZ** and **5,7TzPmPXZ**) showed tricolor-changing MCL behavior in response to a variety of external stimuli, such as grinding, heating, recrystallization, and solvent fuming (yellow–yellowish-orange–orange and yellow–red–deep-red, respectively; Figure 35 b–d). In contrast to the reversible color changes of **5TzPmPXZ** and **7TzPmPXZ** in response to successive grinding and fuming processes (i.e., the grinding of pristine solids caused red-shifts of the emission color and subsequent fuming reverted the emission back to the original colors; Figure 35 b,c), **5,7TzPmPXZ** showed a one-way, two-step red-shift of the emission color in response to a similar set of stimuli (Figure 35 d). OLED devices that were fabricated with the configuration ITO/PEDOT:PSS/emitter in CBP (0.7 wt%)/TmPyPB/Liq/Al showed moderate-to-good EQEs of up to 14.3%.

4.3. TADF- and CPL-Active Materials

The assembly of circularly polarized luminescence (CPL) properties into TADF-active materials would offer tremendous opportunities to develop next-generation emissive materials with applications in highly efficient OLEDs, 3D displays, spintronic devices, information storage/processing, and ellipsometry-based tomography.^[112] However, there is a lack of molecular design strategies for CPL-active organic compounds with high luminescence dissymmetry factors ($g_{lum} = 2(I_L - I_R)/(I_L + I_R)$, where

I_L and I_R are the left and right circularly polarized luminescent intensities, respectively). Typically, the $|g_{lum}|$ values of purely organic compounds are within the range $\times 10^{-5}$ – $\times 10^{-2}$, and only a few examples of this new class of emitting materials have been reported. Yet, achieving both high TADF and CPL characteristics is highly demanding and remains an important challenge in materials science.

In 2015, Hirata and co-workers reported the first example of a TADF- and CPL-active purely organic molecule, **DPHN**, which was constructed from a donor (triphenylamine), an acceptor (naphthalenone), and a chiral carbon center (Figure 36a).^[113]

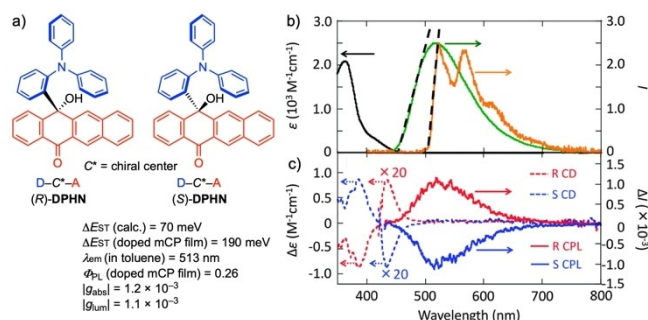


Figure 36. a) Molecular structures and photophysical data of **DPHN**. b) Absorption (black) and PL spectra (green: fluorescence, orange: phosphorescence) of a solution of **DPHN** in toluene. c) Circular dichroism (CD; dotted lines) and CPL (solid lines) spectra of (*R*)- and (*S*)-**DPHN**. Adapted with permission from Ref. [113]. Copyright 2015, Royal Society of Chemistry. mCP = 1,3-bis(9H-carbazol-9-yl)benzene.

DFT calculations suggested that the S_1 state had ICT character, whilst the T_1 state had π - π^* character, which is characteristic of the acceptor unit. The calculated ΔE_{ST} value (70 meV) was much narrower than the experimental one (260 meV in toluene; Figure 36b). CT-based CPL images of pure solutions of the *R*- and *S* enantiomers of **DPHN** in toluene nicely displayed a mirror-image relationship, with a moderate $|g_{lum}|$ value (1.1×10^{-3} ; Figure 36c). The opposite signs of the CD at $\lambda = 386$ nm and the CPL emissions indicated a large conformational change from the ground state to the excited singlet state.

Pieters and co-workers reported a D–A compound with an axially chiral tether, (*R*)-**12** (Figure 37a), which was readily synthesized from tetrafluoro dicyanobenzene, (*R*)-BINOL (1,1'-bi-2-naphthol), and carbazole in high yield as a single enantiomer.^[114] In toluene, the compound exhibited a typical CT absorption band and CT emission bands from $\lambda_{em} = 486$ – 573 nm, depending on the polarity of the solvent (Figure 37c,e). The chiroptical spectra of the *R* and *S* enantiomers were clearly mirror images of each other (Figure 37b,d), thus confirming that the installation of a chiral orthogonal tether unit into the D–A system allowed for CPL. An OLED device that was fabricated with the configuration ITO/CuPc/ α -NPB/TcTa/emitter in mCP (20 wt%)/TmPyPB/LiF/Al (CuPc = copper(II) phthalocyanine, TcTa = tris(4-carbazoyl-9-ylphenyl)amine) showed green EL ($\lambda_{em} \approx 540$ nm) with a maximum power efficiency of 16.3 lm W^{-1} and an EQE of 9.1%. Notably, no racemization occurred after the fabrication of the OLEDs.

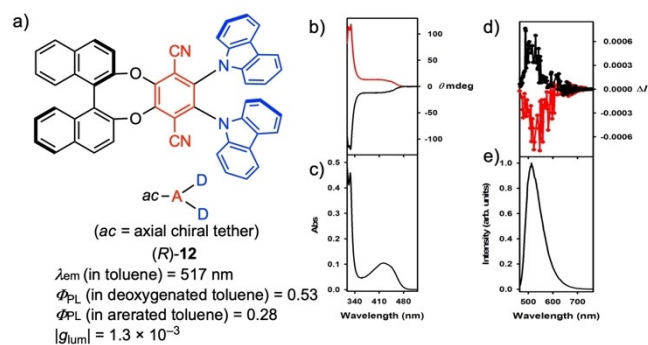


Figure 37. a) Molecular structure of (*R*)-**12**. b–e) CD (b), UV (c), CPL (d), and PL spectra (e) of a solution of (*R*)-**12** in degassed toluene. Adapted with permission from Ref. [114]. Copyright 2016, American Chemical Society.

Thereafter, a similar family of chiral emitting compounds, **BN-CF**, **BN-AF**, **BN-CCN**, and **BN-DCB**, were utilized as CPL-active emitters for circularly polarized organic light-emitting diode (CPOLED) devices by Ma, Tang, and co-workers (Figure 38a).^[115] Interestingly, these compounds were multi-photo-functional, that is, they were AIE active, TADF active, and CPL active. Notably, these chiral compounds showed significantly enhanced $|g_{lum}|$ values in the aggregates compared with their toluene solutions (Figure 38a), which would indicate that the chiral emitters formed chiral aggregates in the solid state. The first small-molecule-based high-performance CPOLEDs were fabricated with the configuration ITO/HATCN/TAPC:HATCN/TcTa/emitter in mCP (10 wt%)/BmPyPB/Liq in BmPyPB (8 wt%)/Liq/Al (BmPyPB = 1,3-bis[3,5-di(pyridin-3-yl)phenyl]benzene), which showed EQEs of up to 9.3% (Figure 38b). The $|g_{EL}|$ value was still as high as 0.016–0.026 for small-molecule-based OLEDs. Again, enhancement of the $|g_{lum}|$ was observed in the non-doped CPOLEDs compared to those of doped CPOLEDs (Figure 38c).

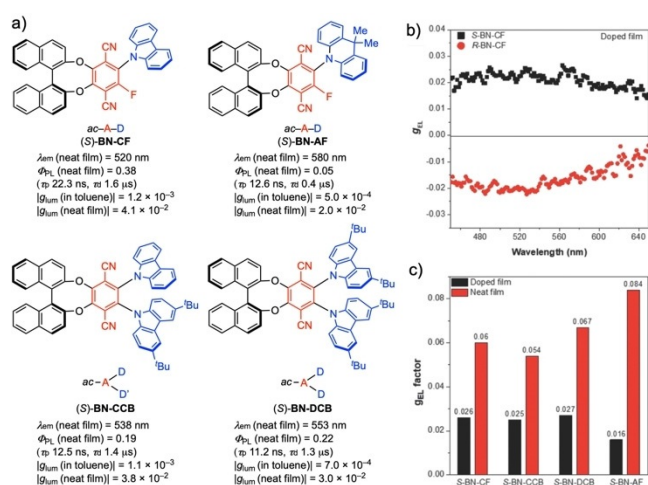


Figure 38. a) Molecular structures of (*S*)-**BN-CF**, (*S*)-**BN-AF**, (*S*)-**BN-CCB**, and (*S*)-**BN-DCB**. b) CPEL profiles of (*S*)- and (*R*)-**BN-CF**. c) Comparison of the $|g_{EL}|$ values of CPOLEDs that were fabricated with doped (black bars) and neat (red bars) emitters. Adapted from Ref. [115].

Fung, Chen, and co-workers developed enantiopure TADF-active CPL emitters **CAI-Cz**, which were comprised of two D-A-D units tethered together by two stereogenic carbon centers (Figure 39a).^[116] Both enantiomers were readily synthesized from enantiopure (*S,S*)- and (*R,R*)-1,2-diaminocyclohexane.

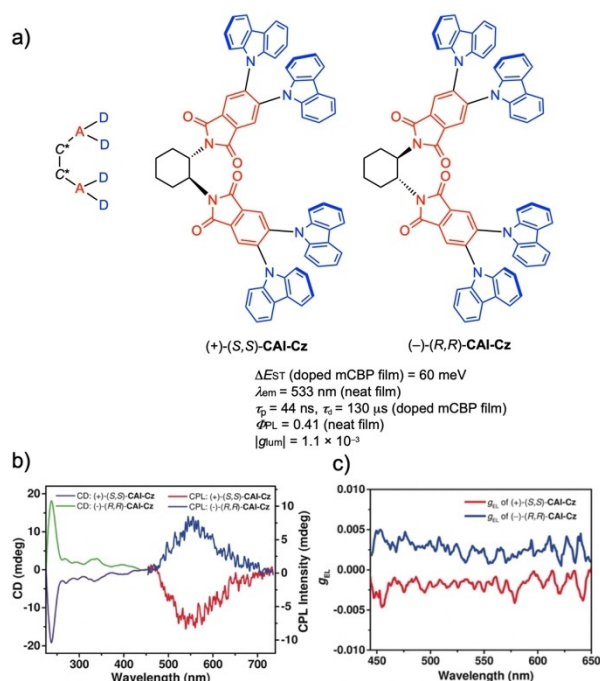


Figure 39. a) Molecular structures and photophysical data of **CAI-Cz**. b) CD and CPL spectra of enantiopure **CAI-Cz**. c) Plots of the g_{EL} values of the emitter-based OLED devices at 9 V. Adapted from Ref. [116].

Emitter-doped mCBP films showed two emitting components in the PL transient decay: a prompt emission ($\tau_p = 44$ ns) and a delayed emission ($\tau_d = 130$ μ s). The CD and CPL spectra of the (+)- and (-)-enantiomers were mirror images of one another (Figure 39b), with a moderate $|g_{lum}|$ value of 1.1×10^{-3} . Circularly polarized OLED devices with the configuration ITO/HATCN/TAPC/TcTa/mCBP/emitter in NPB (15 wt %)/TmPyPB/Liq/Al, which showed green EL ($\lambda_{em} = 520$ nm) with a low turn-on voltage (3.4 V) and a high maximum EQE (19.7%). The circularly polarized electroluminescence (CPEL) profiles were observed by applying enantiopure compounds as the emitter, and showed opposing dissymmetry factors (g_{EL}) of -1.7×10^{-3} and 2.3×10^{-3} for the devices with (+)- and (-)-**CAI-Cz**, respectively.

More recently, Zhao and co-workers developed paracyclophane-structured TADF-active CPL compounds (Figure 40a).^[117] The [2.2]paracyclophane core allowed through-space ICT from the donor (NMe_2) to the acceptor (BMe_2). Notably, both compounds were highly emissive in the solid state ($\Phi_{PL} = 0.53$ for **g-BNMe₂-Cp**; $\Phi_{PL} = 0.33$ for **m-BNMe₂-Cp**). In the deoxygenated toluene solutions, both compounds showed two emissive components with short (prompt fluorescence) and delayed lifetimes (TADF). The CPL spectra for the two enantiomers of **g-BNMe₂-Cp** were mirror images of each other, with a moderate $|g_{lum}|$ value of 4.24×10^{-3} .

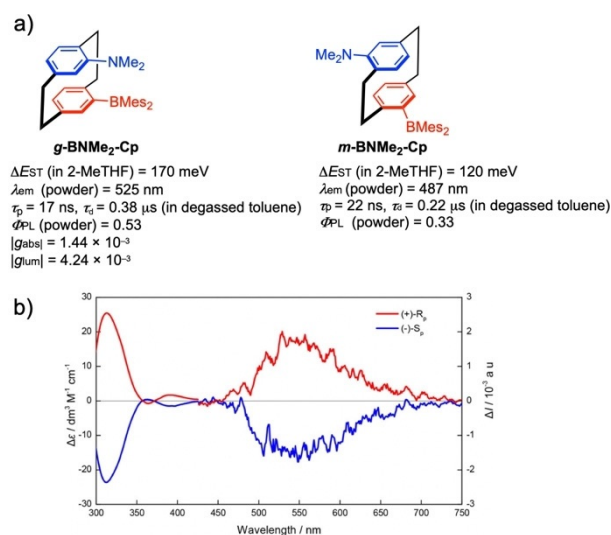


Figure 40. a) Molecular structures and photophysical data of **g-BNMe₂-Cp** and **m-BNMe₂-Cp**. b) CD and CPL spectra of a dilute solution of **g-BNMe₂-Cp** in toluene. Adapted with permission from Ref. [117]. Copyright 2018, American Chemical Society.

As a related topic, very recently, an emitter that showed long-persistent circularly polarized phosphorescence (LPCPP) was developed by Duan and co-workers, by utilizing fully organic ionic crystals.^[118] The crystals were composed of terephthalate (TPA) and (*R*)- or (*S*)-phenylethylammonium (PEA) ion pairs (Figure 41a,b). Upon photoexcitation, the crystals showed prompt blue fluorescence ($\lambda_{em} = 364\text{--}410$ nm) and thereafter long-lived green phosphorescence ($\lambda_{em} = 425\text{--}500$ nm; Figure 41c). Crystals based on enantiomers showed relatively high $|g_{lum}|$ values ($1.5\text{--}2.0 \times 10^{-2}$). Crystallographic analysis of the single crystals revealed that the TPA units formed H-aggregates, which could stabilize the triplet excitons. Notably, the chiral structure of the TPA unit was induced by the chiral environment provided by the PEA units in the crystal, which might have caused the LPCPP.

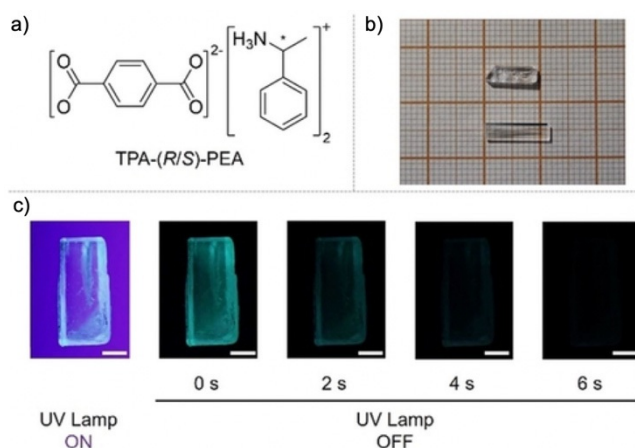


Figure 41. a) Molecular structures of **TPA-(R/S)-PEA**. b) Photographs of **TPA-PEA** crystals. c) Photographs that show the luminescence of the **TPA-PEA** crystal under UV irradiation after photoexcitation for different lengths of time. Adapted from Ref. [118].

5. Summary

In summary, we have described the recent progress in the development of organic emitters, focusing on TADF- and RTP-emitting materials and those that offer multiple functionalities, such as AIE, MCL, and CPL properties. As we have briefly overviewed, research into the designed assembly of multiple emission functions into single organic molecules is still in its infancy. To open up opportunities for the rational design of multifunctional organic emitters for future applications, much deeper understanding of the dynamic photophysical processes of organic molecules in the solid state is required.

Acknowledgements

This work was supported by a Grant-in-Aid for Scientific Research on Innovative Areas “ π -System Figuration: Control of Electron and Structural Dynamism for Innovative Functions” (JSPS KAKENHI; JP15H00997 and JP17H05155 to Y.T.) from the Ministry of Education, Culture, Science and Technology, Japan (MEXT) and by research grants from the Japan Prize Foundation, the Izumi Science and Technology Foundation, the Murata Science Foundation, the Iketani Science and Technology Foundation, the Sasakawa Scientific Research Grant from the Japan Science Society, and Research Encouragement Grants and Continuation Grants for Young Researchers from the Asahi Glass Foundation (to Y.T.). P.D. acknowledges kind support from the First Team Program of the Foundation for Polish Science, co-financed by the European Union under the European Regional Development Fund (First TEAM 2017-4/32). Y.T. and P.D. acknowledge the EU’s Horizon 2020 for funding the OCTA Project (778158).

Conflict of interest

The authors do not declare any conflict of interest.

Keywords: fluorescence · luminescence · materials science · organic emitters · phosphorescence

- [1] H. J. Round, *Electr. World* **1907**, *49*, 309.
- [2] B. H. Soffer, B. B. McFarland, *Appl. Phys. Lett.* **1967**, *10*, 266–267.
- [3] M. Pope, H. P. Kallmann, P. Magnante, *J. Chem. Phys.* **1963**, *38*, 2042–2043.
- [4] B. A. Kamino, Y.-L. Chang, Z.-H. Lu, T. P. Bender, *Org. Electron.* **2012**, *13*, 1479–1485.
- [5] Y. Zhang, M. Song, L. Huang, *J. Lumin.* **2012**, *132*, 2242–2246.
- [6] R. H. Friend, N. C. Greenham in *Handbook of Conducting Polymers, 2nd Revised and Expanded Edition* (Eds.: T. A. Skotheim, R. L. Elsenbaumer, J. R. Reynolds), Marcel Dekker, New York, **1998**, pp. 823–846, “Electroluminescence in Conjugated Polymers”.
- [7] D. F. O’Brien, M. A. Baldo, M. E. Thompson, S. R. Forrest, *Appl. Phys. Lett.* **1999**, *74*, 442–444.
- [8] B. D. Chin, M. C. Suh, M.-H. Kim, S. T. Lee, H. D. Kim, H. K. Chung, *Appl. Phys. Lett.* **2005**, *86*, 133505.
- [9] L. Yang, J.-K. Feng, A.-M. Ren, *J. Org. Chem.* **2005**, *70*, 5987–5996.
- [10] M. Häussler, J. Liu, R. Zheng, J. W. Y. Lam, A. Qin, B. Z. Tang, *Macromolecules* **2007**, *40*, 1914–1925.

- [11] P. Taraneekar, T. Fulghum, D. Patton, R. Ponnampati, G. Clyde, R. Advincula, *J. Am. Chem. Soc.* **2007**, *129*, 12537–12548.
- [12] *Highly Efficient OLEDs with Phosphorescent Materials* (Ed.: H. Yersin), Wiley-VCH, Weinheim, **2008**.
- [13] *Iridium(III) in Optoelectronic and Photonics Applications* (Ed.: E. Zysman-Colman), Wiley, Chichester, **2017**.
- [14] J. E. Yarnell, P. De La Torre, F. N. Castellano, *Eur. J. Inorg. Chem.* **2017**, 5238–5245.
- [15] F. De Angelis, S. Fantacci, N. Evans, C. Klein, S. M. Zakeeruddin, J.-E. Moser, K. Kalyanasundaram, H. J. Bolink, M. Grätzel, M. K. Nazeerudin, *Inorg. Chem.* **2007**, *46*, 5989–6001.
- [16] K. A. King, P. J. Spellane, R. J. Watts, *J. Am. Chem. Soc.* **1985**, *107*, 1431–1432.
- [17] Y. Ohsawa, S. Sprouse, K. A. King, M. K. DeArmond, K. W. Hanck, R. J. Watts, *J. Phys. Chem.* **1987**, *91*, 1047–1054.
- [18] N. Zhao, Y.-H. Wu, H.-M. Wen, X. Zhang, Z.-N. Chen, *Organometallics* **2009**, *28*, 5603–5611.
- [19] H. Xiang, J. Cheng, X. Ma, X. Zhou, J. J. Chruma, *Chem. Soc. Rev.* **2013**, *42*, 6128–6185.
- [20] H. Matsuoka, M. Retegan, L. Schmitt, S. Höger, F. Neese, O. Schiemann, *J. Am. Chem. Soc.* **2017**, *139*, 12968–12975.
- [21] *Physics of Organic Semiconductors* (Ed.: W. Brütting), Wiley-VCH, Weinheim, **2005**.
- [22] C. A. Parker, *Proc. R. Soc. London Ser. A* **1963**, *276*, 125–135.
- [23] C. A. Parker, *Photoluminescence of Solutions: With Applications to Photochemistry and Analytical Chemistry*, 1st ed., Elsevier, Amsterdam, **1968**.
- [24] J. B. Birks, *Rep. Prog. Phys.* **1975**, *38*, 903–974.
- [25] J. Kalinowski, G. Giro, M. Cocchi, V. Fattori, R. Zamboni, *Chem. Phys.* **2002**, *277*, 387–396.
- [26] *Organic Light Emitting Diodes: Principles, Characteristics and Processes* (Ed.: J. Kalinowski), Marcel Dekker, New York, **2005**.
- [27] W. Rettig, *Top. Curr. Chem.* **1994**, *169*, 253–299.
- [28] B. Valuer, M. N. Berberan-Santos, *Molecular Fluorescence: Principles and Applications*, 2nd ed., Wiley-VCH, Weinheim, **2012**.
- [29] F. A. S. Chipem, A. Mishra, G. Krishnamoorthy, *Phys. Chem. Chem. Phys.* **2012**, *14*, 8775–8790.
- [30] J. Kalinowski, M. Cocchi, D. Virgili, V. Fattori, J. A. G. Williams, *Chem. Phys. Lett.* **2007**, *447*, 279–283.
- [31] For reviews on TADF materials, see: a) Y. Tao, K. Yuan, T. Chen, P. Xu, H. Li, R. Chen, C. Zheng, L. Zhang, W. Huang, *Adv. Mater.* **2014**, *26*, 7931–7958; b) Z. Yang, Z. Mao, Z. Xie, Y. Zhang, S. Liu, J. Zhao, J. Xu, Z. Chi, M. P. Aldred, *Chem. Soc. Rev.* **2017**, *46*, 915–1016; c) M. Y. Wong, E. Zysman-Colman, *Adv. Mater.* **2017**, *29*, 1605444.
- [32] H. Uoyama, K. Goushi, K. Shizu, H. Nomura, C. Adachi, *Nature* **2012**, *492*, 234–238.
- [33] F. B. Dias, J. Santos, D. R. Graves, P. Data, R. S. Nobuyasu, M. A. Fox, A. S. Batsanov, T. Palmeira, M. N. Berberan-Santos, M. R. Bryce, A. P. Monkman, *Adv. Sci.* **2016**, *3*, 1600080.
- [34] G. He, O. Schneider, D. Qin, X. Zhou, M. Pfeiffer, K. Leo, *J. Appl. Phys.* **2004**, *95*, 5773–5777.
- [35] F. B. Dias, K. N. Bourdakos, V. Jankus, K. C. Moss, K. T. Kamtekar, V. Bhalla, J. Santos, M. R. Bryce, A. P. Monkman, *Adv. Mater.* **2013**, *25*, 3707–3714.
- [36] V. Jankus, C. J. Chiang, F. Dias, A. P. Monkman, *Adv. Mater.* **2013**, *25*, 1455–1459.
- [37] D. Graves, V. Jankus, F. B. Dias, A. Monkman, *Adv. Funct. Mater.* **2014**, *24*, 2343–2351.
- [38] P. Chen, Q. Peng, L. Yao, N. Gao, F. Li, *Appl. Phys. Lett.* **2013**, *102*, 063301.
- [39] S. Xiang, X. Lv, S. Sun, Q. Zhang, Z. Huang, R. Guo, H. Gu, S. Liu, L. Wang, *J. Mater. Chem. C* **2018**, *6*, 5812–5820.
- [40] Z. R. Grabowski, K. Rotkiewicz, W. Rettig, *Chem. Rev.* **2003**, *103*, 3899–4032.
- [41] W. Rettig, *Angew. Chem. Int. Ed. Engl.* **1986**, *25*, 971–988; *Angew. Chem.* **1986**, *98*, 969–986.
- [42] Y. Suzuki, Q. Zhang, C. Adachi, *J. Mater. Chem. C* **2015**, *3*, 1700–1706.
- [43] A. S. D. Sandanayaka, T. Matsushima, C. Adachi, *J. Phys. Chem. C* **2015**, *119*, 23845–23851.
- [44] C. L. Linfoot, M. J. Leitl, P. Richardson, A. F. Rausch, O. Chepelin, F. J. White, H. Yersin, N. Robertson, *Inorg. Chem.* **2014**, *53*, 10854–10861.

- [45] K. Kawasumi, T. Wu, T. Zhu, H. S. Chae, T. Van Voorhis, M. A. Baldo, T. M. Swager, *J. Am. Chem. Soc.* **2015**, *137*, 11908–11911.
- [46] W. Liu, C.-J. Zheng, K. Wang, Z. Chen, D.-Y. Chen, F. Li, X.-M. Ou, Y.-P. Dong, X.-H. Zhang, *ACS Appl. Mater. Interfaces* **2015**, *7*, 18930–18936.
- [47] K. Shizu, H. Noda, H. Tanaka, M. Taneda, M. Uejima, T. Sato, K. Tanaka, H. Kaji, C. Adachi, *J. Phys. Chem. C* **2015**, *119*, 26283–26289.
- [48] Q. Zhang, J. Li, K. Shizu, S. Huang, S. Hirata, H. Miyazaki, C. Adachi, *J. Am. Chem. Soc.* **2012**, *134*, 14706–14709.
- [49] Q. Zhang, H. Kuwabara, W. J. Potscavage, Jr., S. Huang, Y. Hatae, T. Shibata, C. Adachi, *J. Am. Chem. Soc.* **2014**, *136*, 18070–18081.
- [50] H. Wang, Y. Liu, W. Hu, W. Xu, P. Wang, Y. Wang, X. Luan, *Org. Electron.* **2018**, *61*, 376–382.
- [51] a) P. Data, P. Pander, M. Okazaki, Y. Takeda, S. Minakata, A. P. Monkman, *Angew. Chem. Int. Ed.* **2016**, *55*, 5739–5744; *Angew. Chem.* **2016**, *128*, 5833–5838; b) D. de Sa Pereira, P. L. dos Santos, J. S. Ward, P. Data, M. Okazaki, Y. Takeda, S. Minakata, M. R. Bryce, A. P. Monkman, *Sci. Rep.* **2017**, *7*, 6234.
- [52] J.-X. Chen, K. Wang, C.-J. Zheng, M. Zhang, Y.-Z. Shi, S.-L. Tao, H. Lin, W. Liu, W.-W. Tao, X.-M. Ou, X.-H. Zhang, *Adv. Sci.* **2018**, *5*, 1800436.
- [53] H. F. Higginbotham, P. Pander, R. Rybakiweicz, M. K. Etherington, S. Maniam, M. Zagorska, A. Pron, A. P. Monkman, P. Data, *J. Mater. Chem. C* **2018**, *6*, 8219–8225.
- [54] J. Liang, C. Li, X. Zhuang, K. Ye, Y. Liu, Y. Wang, *Adv. Funct. Mater.* **2018**, *28*, 1707002.
- [55] S.-Y. Lei, J. Zhong, D.-L. Zhou, F.-Y. Zhu, C.-X. Deng, *Chin. Phys. B* **2017**, *26*, 11701.
- [56] G. Schwartz, S. Reineke, T. C. Rosenow, K. Walzer, K. Leo, *Adv. Funct. Mater.* **2009**, *19*, 1319–1333.
- [57] N. Sun, Q. Wang, Y. Zhao, Y. Chen, D. Yang, F. Zhao, J. Chen, D. Ma, *Adv. Mater.* **2014**, *26*, 1617–1621.
- [58] B.-Q. Liu, L. Wang, D.-Y. Gao, J.-H. Zou, H.-L. Ning, J.-B. Peng, Y. Cao, *Light: Sci. Appl.* **2016**, *5*, e16137.
- [59] C. Li, X. Fan, C. Han, H. Xu, *J. Mater. Chem. C* **2018**, *6*, 6747–6754.
- [60] A. Schinabeck, M. J. Leitl, H. Yersin, *J. Phys. Chem. Lett.* **2018**, *9*, 2848.
- [61] For reviews on RTP metal-free organic compounds, see: a) S. Mukherjee, P. Thilagar, *Chem. Commun.* **2015**, *51*, 10988–11003; b) M. Baroncini, G. Bergamini, P. Ceroni, *Chem. Commun.* **2017**, *53*, 2081–2093; c) A. Forni, E. Lucenti, C. Botta, A. Cariatì, *J. Mater. Chem. C* **2018**, *6*, 4603–4626; d) H. Yuasa, S. Kuno, *Bull. Chem. Soc. Jpn.* **2018**, *91*, 223–229.
- [62] J. S. Ward, R. S. Nobuyasu, A. S. Batsanov, P. Data, A. P. Monkman, F. B. Dias, M. R. Bryce, *Chem. Commun.* **2016**, *52*, 2612–2615.
- [63] R. Huang, J. S. Ward, N. A. Kukhta, J. Avó, J. Gibson, T. Penfold, J. C. Lima, A. S. Batsanov, M. N. Berberan-Santos, M. R. Bryce, F. B. Dias, *J. Mater. Chem. C* **2018**, *6*, 9238–9247.
- [64] R. Huang, J. Avó, T. Northey, E. Channing-Pearce, P. L. dos Santos, J. S. Ward, P. Data, M. K. Etherington, M. A. Fox, T. J. Penfold, M. N. Berberan-Santos, J. C. Lima, M. R. Bryce, F. B. Dias, *J. Mater. Chem. C* **2017**, *5*, 6269–6280.
- [65] P. Pander, A. Swist, J. Soloducho, F. B. Dias, *Dyes Pigm.* **2017**, *142*, 315–322.
- [66] P. Pander, A. Swist, R. Turczyn, S. Pouget, D. Djurado, A. Lazauskas, R. Pashazadeh, J. V. Grazulevicius, R. Motyka, A. Klimash, P. J. Skabara, P. Data, J. Soloducho, F. B. Dias, *J. Phys. Chem. C* **2018**, *122*, 24958–24966.
- [67] P. Pander, A. Swist, R. Motyka, J. Soloducho, F. B. Dias, P. Data, *J. Mater. Chem. C* **2018**, *6*, 5434–5443.
- [68] Y. Mu, Z. Yang, J. Chen, Z. Yang, W. Li, X. Tan, Z. Mao, T. Yu, J. Zhao, S. Zheng, S. Liu, Y. Zhang, Z. Chi, J. Xu, M. P. Aldred, *Chem. Sci.* **2018**, *9*, 3782–3787.
- [69] I. Bhattacharjee, N. Acharya, H. Bhatia, D. Ray, *J. Phys. Chem. Lett.* **2018**, *9*, 2733–2738.
- [70] Y. Liu, G. Zhen, P. Fang, Z. Liu, Z. Bian, C. Huang, *J. Mater. Chem. C* **2017**, *5*, 12547–12552.
- [71] T. Serevičius, T. Bučiūnas, J. Bucevičius, J. Dodonova, S. Tumkevičius, K. Kazlauskas, S. Juršėnas, *J. Mater. Chem. C* **2018**, *6*, 11128–11136.
- [72] C. Chen, R. Huang, A. S. Batsanov, P. Pander, Y.-T. Hsu, Z. Chi, F. B. Dias, M. R. Bryce, *Angew. Chem. Int. Ed.* **2018**, *57*, 16407–16411; *Angew. Chem.* **2018**, *130*, 16645–16649.
- [73] C. Zhou, S. Zhang, Y. Gao, H. Liu, T. Shan, X. Liang, B. Yang, Y. Ma, *Adv. Funct. Mater.* **2018**, *28*, 1802407.
- [74] For reviews on AIE materials, see: a) Y. Hong, J. W. Y. Lam, B. Z. Tang, *Chem. Commun.* **2009**, 4332–4353; b) M. Shimizu, T. Hiyama, *Chem. Asian J.* **2010**, *5*, 1516–1531; c) J. Mei, Y. Hong, J. W. Y. Lam, A. Qin, Y. Tang, B. Z. Tang, *Adv. Mater.* **2014**, *26*, 5429–5479; d) J. Mei, N. L. C. Leung, R. T. K. Kwok, J. W. Y. Lam, B. Z. Tang, *Chem. Rev.* **2015**, *115*, 11718–11940; e) Z. He, C. Ke, B. Z. Tang, *ACS Omega* **2018**, *3*, 3267–3277.
- [75] Q. Zhang, D. Tsang, H. Kuwabara, Y. Hatae, B. Li, T. Takahashi, S. Y. Lee, T. Yasuda, C. Adachi, *Adv. Mater.* **2015**, *27*, 2096–2100.
- [76] H. Wang, L. Xie, Q. Peng, L. Meng, Y. Wang, Y. Yi, P. Wang, *Adv. Mater.* **2014**, *26*, 5198–5204.
- [77] S. Xu, T. Liu, Y. Mu, Y.-F. Wang, Z. Chi, C.-C. Lo, S. Liu, Y. Zhang, A. Lien, J. Xu, *Angew. Chem. Int. Ed.* **2015**, *54*, 874–878; *Angew. Chem.* **2015**, *127*, 888–892.
- [78] For a review of ML, which is beyond the scope of this Minireview, see: E. Ubba, Y. Tao, Z. Yang, J. Zhao, L. Wang, Z. Chi, *Chem. Asian J.* **2018**, *13*, 3106–3121.
- [79] S. Gan, W. Luo, B. He, L. Chen, H. Nie, R. Hu, A. Qin, Z. Zhao, B. Z. Tang, *J. Mater. Chem. C* **2016**, *4*, 3705–3708.
- [80] I. Lee, W. Song, J. Y. Lee, *Org. Electron.* **2016**, *29*, 22–26.
- [81] R. Furue, T. Nishimoto, I. S. Park, J. Lee, T. Yasuda, *Angew. Chem. Int. Ed.* **2016**, *55*, 7171–7175; *Angew. Chem.* **2016**, *128*, 7287–7291.
- [82] K.-R. Wee, Y.-J. Cho, S. Jeong, S. Kwon, J.-D. Lee, I.-H. Suh, S. O. Kang, *J. Am. Chem. Soc.* **2012**, *134*, 17982–17990.
- [83] N. V. Nghia, S. Jana, S. Sujith, J. Y. Ryu, J. Lee, S. U. Lee, M. H. Lee, *Angew. Chem. Int. Ed.* **2018**, *57*, 12483–12488; *Angew. Chem.* **2018**, *130*, 12663–12668.
- [84] N. Aizawa, C.-J. Tsou, I. S. Park, T. Yasuda, *Polym. J.* **2017**, *49*, 197–202.
- [85] K. Sun, W. Jiang, X. Ban, B. Huang, Z. Zhang, M. Ye, Y. Sun, *RSC Adv.* **2016**, *6*, 22137–22143.
- [86] K. Matsuoka, K. Albrecht, K. Yamamoto, K. Fujita, *Sci. Rep.* **2017**, *7*, 41780.
- [87] J. Guo, X.-L. Li, H. Nie, W. Luo, S. Gan, S. Hu, R. Hu, A. Qin, Z. Zhao, S.-J. Su, B. Z. Tang, *Adv. Funct. Mater.* **2017**, *27*, 1606458.
- [88] J. Guo, X.-L. Li, H. Nie, W. Luo, R. Hu, A. Qin, Z. Zhao, S.-J. Su, B. Z. Tang, *Chem. Mater.* **2017**, *29*, 3623–3631.
- [89] J. Fan, Y. Zhang, Y. Zhou, L. Lin, C.-K. Wang, *J. Phys. Chem. C* **2018**, *122*, 2358–2366.
- [90] J. Huang, H. Nie, J. Zeng, Z. Zhuang, S. Gan, Y. Cai, J. Guo, S.-J. Su, Z. Zhao, B. Z. Tang, *Angew. Chem. Int. Ed.* **2017**, *56*, 12971–12976; *Angew. Chem.* **2017**, *129*, 13151–13156.
- [91] L. Yu, Z. Wu, G. Xie, W. Zeng, D. Ma, C. Yang, *Chem. Sci.* **2018**, *9*, 1385–1391.
- [92] L. Yu, Z. Wu, G. Xie, C. Zhong, Z. Zhu, D. Ma, C. Yang, *Chem. Commun.* **2018**, *54*, 1379–1382.
- [93] Y. Zhao, W. Wang, C. Gui, L. Fang, X. Zhang, S. Wang, S. Chen, H. Shi, B. Z. Tang, *J. Mater. Chem. C* **2018**, *6*, 2873–2881.
- [94] S. Xiang, Z. Huang, S. Sun, X. Lv, L. Fan, S. Ye, H. Chen, R. Guo, L. Wang, *J. Mater. Chem. C* **2018**, *6*, 11436–11443.
- [95] For reviews on MCL materials, see: a) Y. Sagara, T. Kato, *Nat. Chem.* **2009**, *1*, 605–610; b) Z. Chi, X. Zhang, B. Xu, X. Zhou, C. Ma, Y. Zhang, S. Liu, J. Xu, *Chem. Soc. Rev.* **2012**, *41*, 3878–3896; c) Z. Ma, Z. Wang, M. Teng, Z. Xu, X. Jia, *ChemPhysChem* **2015**, *16*, 1811–1828; d) Y. Sagara, S. Yamane, M. Mitani, C. Weder, T. Kato, *Adv. Mater.* **2016**, *28*, 1073–1095; e) P. Xue, J. Ding, P. Wang, R. Lu, *J. Mater. Chem. C* **2016**, *4*, 6688–6706; f) C. Wang, Z. Li, *Mater. Chem. Front.* **2017**, *1*, 2174–2194.
- [96] In this Minireview, when this term is used, the reversibility of the emission-color change was not confirmed in the referenced papers.
- [97] Z. Xie, C. Chen, S. Xu, J. Li, Y. Zhang, S. Liu, J. Xu, Z. Chi, *Angew. Chem. Int. Ed.* **2015**, *54*, 7181–7184; *Angew. Chem.* **2015**, *127*, 7287–7290.
- [98] B. Xu, Y. Mu, Z. Mao, Z. Xie, H. Wu, Y. Zhang, C. Jin, Z. Chi, S. Liu, J. Xu, Y.-C. Wu, P.-Y. Lu, A. Lien, M. R. Bryce, *Chem. Sci.* **2016**, *7*, 2201–2206.
- [99] H. Tanaka, K. Shizu, H. Nakanotani, C. Adachi, *J. Phys. Chem. C* **2014**, *118*, 15985–15994.
- [100] J. Yang, J. Qin, P. Geng, J. Wang, M. Fang, Z. Li, *Angew. Chem. Int. Ed.* **2018**, *57*, 14174–14178; *Angew. Chem.* **2018**, *130*, 14370–14374.
- [101] P. Ganesan, R. Ranganathan, Y. Chi, X.-K. Liu, C.-S. Lee, S.-H. Liu, G.-H. Lee, T.-C. Lin, Y.-T. Chen, P.-T. Chou, *Chem. Eur. J.* **2017**, *23*, 2858–2866.
- [102] H. Tsujimoto, D.-G. Ha, G. Markopoulos, H. S. Chae, M. A. Baldo, T. M. Swager, *J. Am. Chem. Soc.* **2017**, *139*, 4894–4900.

- [103] B. Huang, Y. Ji, Z. Li, N. Zhou, W. Jiang, Y. Feng, B. Lin, Y. Sun, *J. Lumin.* **2017**, *187*, 414–420.
- [104] B. Huang, Z. Li, H. Yang, D. Hu, W. Wu, Y. Feng, Y. Sun, B. Lin, W. Jiang, *J. Mater. Chem. C* **2017**, *5*, 12031–12034.
- [105] B. Huang, W.-C. Chen, Z. Li, J. Zhang, W. Zhao, Y. Feng, B. Z. Tang, C.-S. Lee, *Angew. Chem. Int. Ed.* **2018**, *57*, 12473–12477; *Angew. Chem.* **2018**, *130*, 12653–12657.
- [106] Z. He, X. Cai, Z. Wang, D. Chen, Y. Li, H. Zhao, K. Liu, Y. Cao, S.-J. Su, *Sci. China Chem.* **2018**, *61*, 677–686.
- [107] M. Okazaki, Y. Takeda, P. Data, P. Pander, H. Higginbotham, A. P. Monkman, S. Minakata, *Chem. Sci.* **2017**, *8*, 2677–2686.
- [108] Y. Takeda, M. Okazaki, S. Minakata, *Chem. Commun.* **2014**, *50*, 10291–10294.
- [109] Y. Takeda, T. Kaihara, M. Okazaki, H. Higginbotham, P. Data, N. Tohnai, S. Minakata, *Chem. Commun.* **2018**, *54*, 6847–6850.
- [110] R. Pashazadeh, P. Pander, A. Lazauskas, F. B. Dias, J. V. Grazulevicius, *J. Phys. Chem. Lett.* **2018**, *9*, 1172–1177.
- [111] X. Zeng, T. Zhou, J. Liu, K. Wu, S. Li, X. Xiao, Y. Zhang, S. Gong, G. Xie, C. Yang, *Adv. Opt. Mater.* **2018**, *6*, 1801071.
- [112] For reviews on CPL, see: a) E. M. Sánchez-Carnerero, A. R. Agarrabeitia, F. Moreno, B. L. Maroto, G. Muller, M. J. Ortiz, S. de la Moya, *Chem. Eur. J.* **2015**, *21*, 13488–13500; b) J. Kumar, T. Nakashima, T. Kawai, *J. Phys. Chem. Lett.* **2015**, *6*, 3445–3452; c) J. Roose, B. Z. Tang, K. S. Wong, *Small* **2016**, *12*, 6495–6512; d) H. Tanaka, Y. Inoue, T. Mori, *ChemPhotoChem* **2018**, *2*, 386–402.
- [113] T. Imagawa, S. Hirata, K. Totani, T. Watanabe, M. Vacha, *Chem. Commun.* **2015**, *51*, 13268–13271.
- [114] S. Feuillastre, M. Pauton, L. Gao, A. Desmarchelier, A. J. Riives, D. Prim, D. Tondelier, B. Geffroy, G. Muller, G. Clavier, G. Pieters, *J. Am. Chem. Soc.* **2016**, *138*, 3990–3993.
- [115] F. Song, Z. Xu, Q. Zhang, Z. Zhao, H. Zhang, W. Zhao, Z. Qiu, C. Qi, H. Zhang, H. H. Y. Sung, I. D. Williams, J. W. Y. Lam, Z. Zhao, A. Qin, D. Ma, B. Z. Tang, *Adv. Funct. Mater.* **2018**, *28*, 1800051.
- [116] M. Li, S.-H. Li, D. Zhang, M. Cai, L. Duan, M.-K. Fung, C.-F. Chen, *Angew. Chem. Int. Ed.* **2018**, *57*, 2889–2893; *Angew. Chem.* **2018**, *130*, 2939–2943.
- [117] M.-Y. Zhang, Z.-Y. Li, B. Lu, Y. Wang, Y.-D. Ma, C.-H. Zhao, *Org. Lett.* **2018**, *20*, 6868–6871.
- [118] W. Chen, Z. Tian, Y. Li, Y. Jiang, M. Liu, P. Duan, *Chem. Eur. J.* **2018**, *24*, 17444–17448.

Manuscript received: December 5, 2018

Accepted manuscript online: January 4, 2019

Version of record online: January 28, 2019